Available online at www.eccomasproceedia.org
Eccomas Proceedia COMPDYN (2021) 1892-1921

ECCOMAS
Proceedia

COMPDYN 2021
8th ECCOMAS Thematic Conference on
Computational Methods in Structural Dynamics and Earthquake Engineering
M. Papadrakakis, M. Fragiadakis (eds.)
Streamed from Athens, Greece, 28 - 30 June 2021

DISPERSION ANALYSIS OF BULK ACOUSTIC WAVES IN PIEZOELECTRIC MEDIA DISCRETIZED BY ENERGY-ORTHOGONAL FINITE ELEMENTS

Francisco J. Brito Castro

Departamento de Ingeniería Industrial, Universidad de La Laguna
Calle Méndez Núñez 67-2C, Santa Cruz de Tenerife 38001, Spain
e-mail: fjbrito@ull.edu.es

Abstract

This contribution studies the propagation of bulk acoustic waves in piezoelectric media discretized by the finite element method. The element elastic and dielectric stiffness matrices are split into basic and higher order components which are related to the mean and deviatoric components of the element strain and electric fields, respectively. This decomposition is applied to the total energy of the finite element assemblage. By a dispersion analysis the higher order total energy is related to the total energy error for the propagating waves. An averaged correlation is proposed as an error indicator for the finite element vibration eigenmodes in piezoelectric solids.

Keywords: energy-orthogonal stiffness, numerical dispersion, piezoelectric media, vibration eigenmodes.

ISSN:2623-3347
Peer-review under responsibility of the organizing committee of COMPDYN 2021.
doi:10.7712/120121.8610.18518

1 INTRODUCTION

It is well known that the wave scattering at boundaries creates an interference field that, if composed solely of waves of frequency equal to a natural frequency of the bounded medium, takes the form of a standing-wave field which is an eigenmode of the continuum [1]. For homogeneous piezoelectric solids, whose three dimensions are comparable, this standing-wave field could be considered essentially composed of propagating quasi-longitudinal and quasi-shear bulk acoustic waves. In this case the goal of determining the finite element mesh required to accurately represent a given number of eigenmodes could be approached by analysing the effect of the spatial discretization over the propagation of such bulk acoustic waves in unbounded media. This effect becomes apparent by observing the dispersive behavior of the waves, a phenomenon that is not present in the physical system [2]. This contribution extends the author's previous research about homogeneous isotropic elastic solids [3].

The piezoelectric media covered in this research include PZT (Lead zirconate titanate ($Pb(Zr,Ti)O_3$)) piezoceramics [4]. These are transversely isotropic and they behave the same as crystals in class Hexagonal (6mm). The poling direction is supposed along the Z-axis. The material constants for the piezoceramics selected (PZT-5H, PZT-8 and PZT-5A) can be found in reference [5]. Also PMN-PT (Lead magnesium niobate-lead titanate ($Pb(Mg_{1/3}Nb_{2/3})O_3$-$PbTiO_3$)) <001> poled single crystals are covered [6]: the single crystal PMN-30PT from reference [7], and the commercial grade single crystals PMN-31PT and PIN-PMN-PT (TRS X2B and TRS X4B) from TRS Technologies Inc. [8] have been selected. These single crystals exhibit Tetragonal (4mm) symmetry in macroscopic material properties. See Appendix 1 for the material constants of the PZT piezoceramics and PMN-PT single crystals selected.

An enlightening discussion about PZT piezoceramics and PMN-PT single crystals in the context of sonar applications can be found in reference [9].

1.1 Finite element formulation

In a lossless piezoelectric medium discretized by the finite element method the equations of equilibrium governing its linear dynamic response for time-harmonic waves will be [10],

$$\begin{pmatrix} \mathbf{K}_{uu} - \omega^2\mathbf{M} & \mathbf{K}_{u\phi} \\ -\mathbf{K}_{\phi u} & \mathbf{K}_{\phi\phi} \end{pmatrix} \begin{pmatrix} \mathbf{x} \\ \boldsymbol{\phi} \end{pmatrix} = \begin{pmatrix} \mathbf{F} \\ \mathbf{Q} \end{pmatrix}, \quad \mathbf{K}_{\phi u} = \mathbf{K}_{u\phi}^T; \quad \begin{matrix} \mathbf{x} = \tilde{\mathbf{x}}\exp(-i\omega t), & \mathbf{F} = \tilde{\mathbf{F}}\exp(-i\omega t) \\ \boldsymbol{\phi} = \tilde{\boldsymbol{\phi}}\exp(-i\omega t), & \mathbf{Q} = \tilde{\mathbf{Q}}\exp(-i\omega t) \end{matrix} \tag{1}$$

where: $\mathbf{M}$, consistent mass matrix; $\mathbf{K}_{uu}$ ($\mathbf{K}_{\phi\phi}$, $\mathbf{K}_{u\phi}$), elastic (dielectric, piezoelectric) stiffness matrix of the finite element assemblage; $\tilde{\mathbf{x}}$ ($\tilde{\mathbf{F}}$, $\tilde{\boldsymbol{\phi}}$, $\tilde{\mathbf{Q}}$), column matrix containing the complex amplitude of the nodal displacements (external loads, electric potentials, free electric charges); $\omega = 2\pi/T$, circular frequency; T, period of wave; t, time.

The total energy will be equal to the sum of pure elastic energy and pure electric energy [11],

$$E^M = \tfrac{1}{2}\mathrm{Re}[\mathbf{x}^T]\mathbf{K}_{uu}\,\mathrm{Re}[\mathbf{x}] \quad (a) \qquad E^E = \tfrac{1}{2}\mathrm{Re}[\boldsymbol{\phi}^T]\mathbf{K}_{\phi\phi}\,\mathrm{Re}[\boldsymbol{\phi}] \quad (b) \tag{2}$$

At element level

$$\begin{aligned} \mathbf{K}_{uu}^e &= \int_{Ve}\mathbf{B}_u^T[\mathbf{C}^E]\mathbf{B}_u dV \quad (a) & \mathbf{K}_{\phi\phi}^e &= \int_{Ve}\mathbf{B}_\phi^T[\boldsymbol{\varepsilon}^S]\mathbf{B}_\phi dV \quad (b) \\ \mathbf{K}_{u\phi}^e &= \int_{Ve}\mathbf{B}_u^T[\mathbf{e}]^T\mathbf{B}_\phi dV \quad (c) & \mathbf{K}_{\phi u}^e &= \int_{Ve}\mathbf{B}_\phi^T[\mathbf{e}]\mathbf{B}_u dV \quad (d) \end{aligned} \tag{3}$$

where: $\mathbf{B}_u$ ($\mathbf{B}_\phi$), matrix relating the strain components (gradient of electric potential) to the nodal values of displacement (electric potential); $\mathbf{C}^E$, elasticity matrix evaluated at constant electric field; $\boldsymbol{\varepsilon}^S$, dielectric matrix evaluated at constant mechanical strain; $\mathbf{e}$, piezoelectric matrix.

If the matrices $\mathbf{B}_u$ and $\mathbf{B}_\phi$ are partitioned into mean and deviatoric components,

$$\begin{aligned} &\mathbf{B}_u = \overline{\mathbf{B}}_u + \mathbf{B}_{u,d}; \quad \overline{\mathbf{B}}_u V^e = \int_{Ve} \mathbf{B}_u dV, \quad \mathbf{B}_{u,d} = \mathbf{B} - \overline{\mathbf{B}}_u \quad (a) \\ &\mathbf{B}_\phi = \overline{\mathbf{B}}_\phi + \mathbf{B}_{\phi,d}; \quad \overline{\mathbf{B}}_\phi V^e = \int_{Ve} \mathbf{B}_\phi dV, \quad \mathbf{B}_{\phi,d} = \mathbf{B} - \overline{\mathbf{B}}_\phi \quad (b) \end{aligned} \tag{4}$$

the matrices Eq. (3a) and Eq. (3b) would be respectively decomposed as addition of basic and higher order components,

$$\begin{aligned} &\mathbf{K}^e_{uu} = \mathbf{K}^e_{uu,b} + \mathbf{K}^e_{uu,h}; \quad \mathbf{K}^e_{uu,b} = \overline{\mathbf{B}}^T_u [\mathbf{C}^E] \overline{\mathbf{B}}_u V^e, \quad \mathbf{K}^e_{uu,h} = \int_{Ve} \mathbf{B}^T_{u,d} [\mathbf{C}^E] \mathbf{B}_{u,d} dV \quad (a) \\ &\mathbf{K}^e_{\phi\phi} = \mathbf{K}^e_{\phi\phi,b} + \mathbf{K}^e_{\phi\phi,h}; \quad \mathbf{K}^e_{\phi\phi,b} = \overline{\mathbf{B}}^T_\phi [\boldsymbol{\varepsilon}^S] \overline{\mathbf{B}}_\phi V^e, \quad \mathbf{K}^e_{\phi\phi,h} = \int_{Ve} \mathbf{B}^T_{\phi,d} [\boldsymbol{\varepsilon}^S] \mathbf{B}_{\phi,d} dV \quad (b) \end{aligned} \tag{5}$$

In this case it is said that the element stiffness matrices are formulated in energy-orthogonal form [12]. The decomposition in Eq. (5) holds for the complete model,

$$\mathbf{K}_{uu} = \mathbf{K}_{uu,b} + \mathbf{K}_{uu,h} \quad (a) \quad \mathbf{K}_{\phi\phi} = \mathbf{K}_{\phi\phi,b} + \mathbf{K}_{\phi\phi,h} \quad (b) \tag{6}$$

For a stationary wave the amplitudes of nodal displacements and electric potentials are real-valued vectors in Eq. (1). Then, from Eq. (2a) and Eq. (2b), the period-averaged elastic and electric energies for the discretized domain will be, respectively,

$$\overline{E}^M = \tfrac{1}{4} \tilde{\mathbf{x}}^T \mathbf{K}_{uu} \tilde{\mathbf{x}} \quad (a) \quad \overline{E}^E = \tfrac{1}{4} \tilde{\boldsymbol{\phi}}^T \mathbf{K}_{\phi\phi} \tilde{\boldsymbol{\phi}} \quad (b) \tag{7}$$

By introducing Eq. (6) into Eq. (7), the basic and higher order period-averaged energies will be obtained. The latter components will be

$$\overline{E}^M_h = \tfrac{1}{4} \tilde{\mathbf{x}}^T \mathbf{K}_{uu,h} \tilde{\mathbf{x}} \quad (a) \quad \overline{E}^E_h = \tfrac{1}{4} \tilde{\boldsymbol{\phi}}^T \mathbf{K}_{\phi\phi,h} \tilde{\boldsymbol{\phi}} \quad (b) \tag{8}$$

2 DISPERSION ANALYSIS

The unbounded piezoelectric domain is discretized by a regular mesh of finite elements. Two different isoparametric finite elements with consistent mass matrix are considered: the hexahedron with twenty nodes and brick geometry HE20, Fig. 1, and the pentahedron with fifteen nodes and right prismatic isosceles geometry PE15, Fig. 2 [13]. The nodal lattice formed by the finite element assemblage has four and five nodes per unit cell, respectively. Different meshes with the same element volume can be selected by the aspect ratio parameter, $0 < \gamma \leq 1$; the skew angle, $0 \leq \beta < 90^o$ (only HE 20 element); and the distortion-Z parameter, $\varepsilon > 0$.

For uniform plane harmonic bulk waves at the continuum piezoelectric medium, the displacement vector field and the electric potential field will be, respectively,

$$\mathbf{u} = A^u \hat{\mathbf{a}} \exp(i\kappa \mathbf{n} \cdot \mathbf{r}) \exp(-i\omega t) \quad (a) \quad \phi = A^\phi e \exp(i\kappa \mathbf{n} \cdot \mathbf{r}) \exp(-i\omega t) \quad (b) \tag{9}$$

where: A^u and A^ϕ, amplitudes of the wave; $\hat{\mathbf{a}}$, polarization vector; $\mathbf{n}$, wave normal, unit vector indicating the direction of the wave propagation; $\mathbf{r}$, position vector; $\kappa = 2\pi/\lambda = \omega/c$, wave number; λ, wavelength; c, phase velocity at the continuum medium.

The wave normal has the components $n_1 = \cos\phi\sin\theta$, $n_2 = \sin\phi\sin\theta$ and $n_3 = \cos\theta$, where: ϕ, azimuthal angle, $0 \leq \phi \leq 180^o$; θ, polar angle, $0 \leq \theta \leq 180^o$, Fig. 1.

The polarization vectors and phase velocities are solution of the stiffened Christoffel equation, which is expressed in abbreviated subscript notation [14],

$$(l_{iK}(C^E_{KL} + [e_{Kj} n_j][n_i e_{iL}] / (n_i \varepsilon^S_{ij} n_j)) l_{Lj}) \hat{a}_j = \rho c^2 \hat{a}_i, \quad i, j = 1, \ldots, 3; \quad K, L = 1, \ldots, 6 \tag{10}$$

where the non-null values of l_{iK} are: $l_{11} = n_1$, $l_{15} = n_3$, $l_{16} = n_2$, $l_{22} = n_2$, $l_{24} = n_3$, $l_{26} = n_1$, $l_{33} = n_3$, $l_{34} = n_2$, and $l_{35} = n_1$.

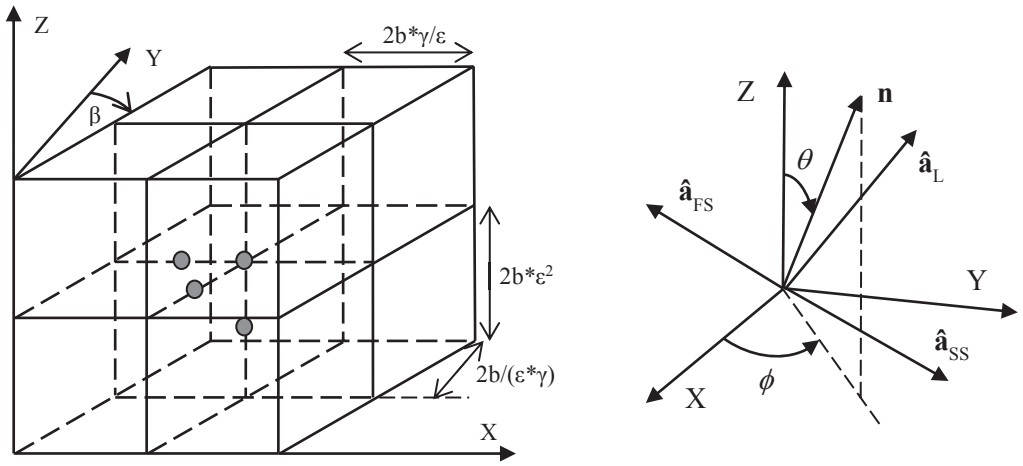

Figure 1: Piezoelectric domain discretized by a regular mesh of HE20 elements and unit cell with four nodes. Polarization vectors.

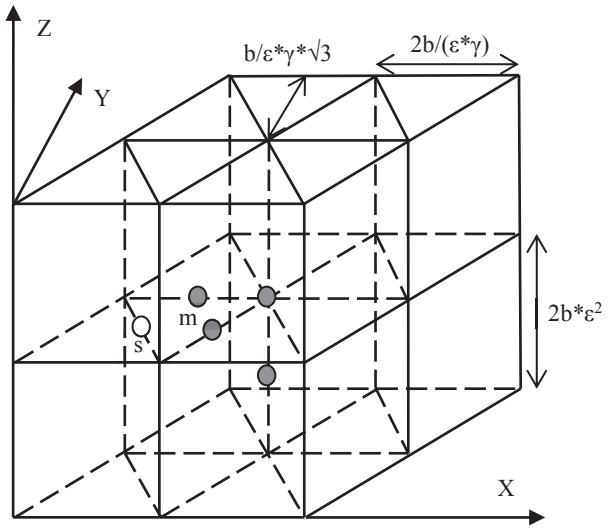

Figure 2: Piezoelectric domain discretized by a regular mesh of PE15 elements and unit cell with four master nodes (m) and one slave node (s).

By solving the eigenproblem Eq. (10), three mutually orthogonal waves at the continuum medium are computed, Fig. 1: ($\hat{\mathbf{a}}_{SS}$, c_{SS}), slow quasi-shear wave, SS; ($\hat{\mathbf{a}}_{FS}$, c_{FS}), fast quasi-shear wave, FS; and ($\hat{\mathbf{a}}_{L}$, c_{L}), quasi-longitudinal wave, L.

Then, the electric potential at the continuum medium can be computed for each wave,

$$A^{\phi} = A^{u}(n_i e_{iK} l_{Kj} \big/ (n_i \varepsilon_{ij}^{S} n_j)\hat{a}_j), \quad i,j = 1,\ldots,3; \quad K = 1,\ldots,6 \tag{11}$$

For the displacement vector field Eq. (9a) and for the electric potential field Eq. (9b), the densities of period-averaged pure elastic energy and period-averaged pure electric energy at the continuum medium can be respectively computed by the equations [14]

$$\bar{E}_0^{M} = \tfrac{1}{4}\omega^2 (A^{u})^2 \, l_{Ki}\hat{a}_i C_{KL}^{E} l_{Lj}\hat{a}_j \big/ c^2 \quad (a) \quad \bar{E}_0^{E} = \tfrac{1}{4}\omega^2 (A^{\phi})^2 \, n_i \varepsilon_{ij}^{S} n_j \big/ c^2 \quad (b) \tag{12}$$

2.1 Characteristic equations

The characteristic equations can be found assuming harmonic waves Eq. (9) with different amplitudes in each node of the unit cell,

$$\tilde{\mathbf{u}} = A_j^u \hat{\mathbf{a}} \exp(i\kappa \mathbf{n}\cdot\mathbf{r}) \quad (a) \quad \tilde{\phi} = A_j^\phi e \exp(i\kappa \mathbf{n}\cdot\mathbf{r}) \quad (b); \quad j = 1,\ldots,N \tag{13}$$

where: N, number of nodes per unit cell.

Inserting the solutions Eq. (13) into the homogeneous part of Eq. (1), the characteristic equation for each node of the unit cell is yielded by equilibrium of nodal forces into the direction of the particle displacement [15],

$$\mathbf{F}_K^{uu}\cdot\hat{\mathbf{a}} - \omega^2 \mathbf{F}_M \cdot \hat{\mathbf{a}} + \mathbf{F}_K^{u\phi}\cdot\hat{\mathbf{a}} = 0, \quad -F_K^{\phi u} + F_K^{\phi\phi} = 0 \tag{14}$$

By considering Eq. (14) for each node of the unit cell, a homogeneous system of $2N$ algebraic equations is formed,

$$\begin{pmatrix} \mathbf{a}^{uu}(m,\phi,\theta,\boldsymbol{\alpha}) + \varpi^2 \mathbf{b}^{uu}(m,\phi,\theta,\boldsymbol{\alpha}) & \mathbf{a}^{u\phi}(m,\phi,\theta,\boldsymbol{\alpha}) \\ \mathbf{a}^{\phi u}(m,\phi,\theta,\boldsymbol{\alpha}) & \mathbf{a}^{\phi\phi}(m,\phi,\theta,\boldsymbol{\alpha}) \end{pmatrix} \begin{pmatrix} \mathbf{A}^u \\ \mathbf{A}^\phi \end{pmatrix} = \begin{pmatrix} \mathbf{0} \\ \mathbf{0} \end{pmatrix} \tag{15}$$

$$m = b\kappa/\pi = 2b/\lambda, \quad \varpi = (2b/c)\omega \tag{16}$$

where: m, dimensionless wave number, $0 < m < 1$; b, half of the element size; ϖ, dimensionless frequency of the discretized piezoelectric medium; $\boldsymbol{\alpha} = (\gamma, \beta, \varepsilon)$ form parameter for HE20 mesh, or $\boldsymbol{\alpha} = (\gamma, \varepsilon)$ form parameter for PE15 mesh.

In this procedure both the global stiffness matrices and the global mass matrix have been expressed in a suitable form,

$$\mathbf{K}_{xx} = \rho c^2 (2b)\mathbf{K}_{xx}^0 \quad xx = (uu, u\phi, \phi u, \phi\phi), \quad \mathbf{M} = \rho (2b)^3 \mathbf{M}^0 \tag{17}$$

The homogeneous system of $2N$ algebraic equations Eq. (15) can be reduced to a homogeneous system of N equations by static condensation [16]. So, from Eq. (15),

$$(\mathbf{a}^{uu} + \varpi^2 \mathbf{b}^{uu})\mathbf{A}^u + \mathbf{a}^{u\phi}\mathbf{A}^\phi = \mathbf{0} \quad (a) \quad \mathbf{A}^\phi = -(\mathbf{a}^{\phi\phi})^{-1}\mathbf{a}^{\phi u}\mathbf{A}^u \quad (b) \tag{18}$$

Inserting Eq. (18b) into (18a), the condensate system of characteristic equations is formed,

$$(\mathbf{a}^{uu} - \mathbf{a}^{u\phi}(\mathbf{a}^{\phi\phi})^{-1}\mathbf{a}^{\phi u} + \varpi^2 \mathbf{b}^{uu})\mathbf{A}^u = \mathbf{0} \quad \Leftrightarrow \quad \mathbf{Z}\mathbf{A}^u = \mathbf{0} \tag{19}$$

2.2 Dispersion equations

The system of homogeneous algebraic equations given in Eq. (19) has a non-trivial solution only if the matrix **Z** is singular; that is, det [**Z**] = 0. Then it is yielded the following polynomial equation which is called the characteristic frequency equation for the plane wave propagation,

$$\sum_{r=0}^{N} c_r(m,\phi,\theta,\boldsymbol{\alpha})\varpi^{2r} = 0, \quad c_N = 1 \tag{20}$$

It is an important fact that the N zeroes of a polynomial of degree $N \geq 1$ with complex coefficients depend continuously upon the coefficients [17]. Thus, sufficiently small changes in the coefficients of a polynomial can lead only to small changes in any zero. However, if the zeros are numerically computed, there is no simple way to define a function which takes the N coefficients (all but the leading 1) of a monic polynomial of degree N to the N zeroes of the polynomial, since there is no natural way to define an ordering among the N zeroes. In the case of the HE20 mesh, for which the polynomial Eq. (20) is quartic, the above difficulty has been

overcome by computing the zeroes in closed form as functions of its coefficients. Then, the components

$$\varpi_k = \varpi_k(m,\phi,\theta,\boldsymbol{\alpha}), \quad k=1,\ldots,4 \tag{21}$$

will be continuous functions precisely defined. They are called the dispersion equations.

Substituting Eq. (21) into Eq. (19), the displacement wave amplitudes corresponding to the nodes of the unit cell are yielded for each dispersion equation. Then, by Eq. (18b), the corresponding electric potential amplitudes are recovered.

To find the zeros of a polynomial equation as functions of its coefficients beyond the quartic equation is a very difficult mathematical problem [18]. Then, for the mesh PE15 which has five nodes per unit cell, if the zeros of Eq. (20) are numerically computed, the above mentioned ordering difficulty could be a problem. In this case, by considering the initial condition,

$$\lim_{m\to 0}\varpi_1(m,\phi,\theta,\boldsymbol{\alpha}) = 0 \tag{22}$$

it is proposed to compute the first dispersion equation by a reduced unit cell obtained by a procedure of exact dynamic condensation [16].

Assume that the total nodes at the unit cell are categorized as master nodes (m) and slave nodes (s), where the number of master nodes is four and the number of slave nodes is one, Fig 2. With this arrangement, the system of characteristic equations Eq. (19) may be partitioned as

$$\begin{pmatrix} \mathbf{Z}_{mm}(q) & \mathbf{Z}_{ms}(q) \\ \mathbf{Z}_{sm}(q) & \mathbf{Z}_{ss}(q) \end{pmatrix} \begin{pmatrix} \mathbf{A}_m^u \\ \mathbf{A}_s^u \end{pmatrix} = \begin{pmatrix} \mathbf{0} \\ \mathbf{0} \end{pmatrix}, \quad q = \varpi^2 \tag{23}$$

From Eq. (23) the relation of wave amplitudes between the master and slave nodes may be obtained as

$$\mathbf{A}_s^u = -\mathbf{Z}_{ss}^{-1}(q)\mathbf{Z}_{sm}(q)\mathbf{A}_m^u \tag{24}$$

Then, by back-substituting, the system of characteristic equations of the reduced unit cell is obtained as

$$\mathbf{Z}_R(q)\mathbf{A}_m^u = \mathbf{0}, \quad [\mathbf{K}_R(q) + q\mathbf{M}_R(q)]\mathbf{A}_m^u = \mathbf{0} \tag{25}$$

Then, from Eq. (25), the reduced form of the characteristic frequency equation is obtained

$$q^4 + c_{3R}q^3 + c_{2R}q^2 + c_{1R}q + c_{0R} = 0, \quad c_{rR}(m,\phi,\theta,\boldsymbol{\alpha},q), \quad r=0,\ldots,3 \tag{26}$$

The first dispersion equation is computed by the following iterative procedure:

Set by Eq. (22) the initial value $q_{i1} = 0$.

Do for $0 < m < 1$, step Δm

1. Compute the coefficients $c_{rR}(m,\phi,\theta,\boldsymbol{\alpha},q_{i1})$ of Eq. (26).
2. Compute the zero q_1 of the quartic polynomial Eq. (26).

Do while ($|(q_1 - q_{i1})/q_1| \geq \delta$)

1. Refresh initial value $q_{i1} = q_1$.
2. Compute the coefficients $c_{rR}(m,\phi,\theta,\boldsymbol{\alpha},q_{i1})$ of Eq. (26).
3. Compute the zero q_1 of the quartic polynomial Eq. (26).

End do

3. Substituting q_1 into Eq. (25) to compute the wave amplitudes at the master nodes.

4. Substituting q_1 into Eq. (24) to compute the wave amplitudes at the slave nodes.

5. Refresh initial value $q_{i1} = q_1$ for the next step.

End do

It must be recall the equality of the energy and group velocities for bulk acoustic waves in a lossless piezoelectric medium [19], and the equality of the normal component of the group velocity and the phase velocity at the anisotropic continuum [20]. Then, the indicators of numerical dispersion for the phase velocity and the normal component of the group velocity are yielded for each dispersion equation. From Eq. (16),

$$e_p = c_p/c = (2\pi)^{-1}\,\varpi/m \quad (a) \quad e_{gn} = c_{gn}/c = (2\pi)^{-1}\,\partial\varpi/\partial m \quad (b) \tag{27}$$

The range of dimensionless wave number values where each dispersion equation represents the propagation of acoustic waves in the discretized medium will be called the acoustical branch of the dispersion equation. In order to determine the acoustical branches the following constraint conditions are imposed,

$$A_1^u = 1, \quad A_j^u(m,\phi,\theta,\boldsymbol{\alpha}) > 0 \quad j = 2,\ldots,N \quad (a) \quad \left(\partial\varpi/\partial m\right)_{\phi,\theta,\boldsymbol{\alpha}} > 0 \quad (b) \tag{28}$$

In molecular physics the condition Eq. (28a) is called the restriction of the lattice spectrum to the acoustical branch [21]. By considering Eq. (27b), the constraint condition Eq. (28b) imposes that the normal component of the group velocity or energy velocity must have the wave direction. The preliminary constraint condition dim [**N**(**Z**)] = 1, over the dimension of the null space of matrix **Z** for the HE20 mesh, or dim [**N**($\mathbf{Z}_R$)] = 1 for the PE15 mesh, must be imposed in order to Eq. (28a) would be a meaningful constraint condition. For each dispersion equation only the acoustical branch will be considered.

2.3 Energy at the unit cell

From Eq. (2), Eq. (16) and Eq. (17), the densities of period-averaged elastic and electric energies at the unit cell are computed,

$$\begin{aligned} \bar{E}^M &= \tfrac{1}{2}\rho(\omega/\varpi)^2 C\int_0^1 \mathrm{Re}[\tilde{\mathbf{x}}^T \exp(-i2\pi\tau)]\,\mathrm{Re}[\tilde{\mathbf{F}}_{uu}^0 \exp(-i2\pi\tau)]d\tau \quad (a) \\ \bar{E}^E &= \tfrac{1}{2}\rho(\omega/\varpi)^2 C\int_0^1 \mathrm{Re}[\tilde{\boldsymbol{\phi}}^T \exp(-i2\pi\tau)]\,\mathrm{Re}[\tilde{\mathbf{F}}_{\phi\phi}^0 \exp(-i2\pi\tau)]d\tau \quad (b) \end{aligned} \tag{29}$$

where: $\tau = t/T$, $0 \le \tau \le 1$, dimensionless time; $\tilde{\mathbf{F}}_{uu}^0$ and $\tilde{\mathbf{F}}_{\phi\phi}^0$ are column matrices of forces at the nodes of the unit cell; C = 1 for the HE20 mesh, $C = 2/(3)^{1/2}$ for the PE15 mesh.

From the decomposition in Eq. (6), the above computed densities of period-averaged energies Eq. (29) can be partitioned as addition of basic and higher order components. Then, the percentage of period-averaged higher order total energy can be defined as

$$e_h = (\bar{E}_h^M + \bar{E}_h^E)/(\bar{E}^M + \bar{E}^E) = \bar{E}_h/\bar{E}, \quad e_h = e_h(m,\phi,\theta,\boldsymbol{\alpha}) \tag{30}$$

From Eq. (29) and Eq. (12), the percentage indicator of total energy error associated with the spatial discretization that is introduced by the finite element model is defined as

$$e_T = ((\bar{E}^M + \bar{E}^E)/(\bar{E}_0^M + \bar{E}_0^E)) - 1 = (\bar{E}/\bar{E}_0) - 1, \quad e_T = e_T(m,\phi,\theta,\boldsymbol{\alpha}) \tag{31}$$

From Eq. (30) and Eq. (31), a mapping between the total energy error and the percentage of higher order total energy can be also computed,

$$e_T = e_T(e_h,\phi,\theta,\boldsymbol{\alpha}) \tag{32}$$

2.4 Substitute wave field

It is clear that the harmonic acoustic waves cannot be exactly captured by a regular mesh of finite elements HE20 or PE15. This fact is a consequence of the element interpolation which is quadratic. A substitute wave field [22] or alias field [13] has been obtained in the discretized unbounded medium by performing a dispersion analysis in terms of allowable polarizations of the continuum. The substitute wave field is obtained by collocating Eq. (13a) and Eq. (13b) in each node of the unit cell. The assumption of different amplitudes is introduced because the equation of equilibrium is different for each node. The analysis yields the relative wave amplitudes and the dispersion relation under which the alias field may propagate in the discretized medium. The alias wave field will be

$$\tilde{\mathbf{u}}^a = \sum N_{S,i} \tilde{\mathbf{u}}_i, \quad \tilde{\phi}^a = \sum N_{S,i} \tilde{\phi}_i \tag{33}$$

where: $\tilde{\mathbf{u}}_i$, the values of Eq. (13a) at the nodes; $\tilde{\phi}_i$, the values of Eq. (13b) at the nodes; $N_{S,i}$, the nodal shape functions.

By computing the wave amplitude distortion, the discretization error of the wave field Eq. (33) can be decomposed as addition of interpolation and pollution errors [23].

2.5 Numerical research

For the waves and media considered the indicators Eq. (27), Eq. (30) and Eq. (31) are computed versus dimensionless wave number for different meshes and directions of wave propagation. Five meshes having the same element volume will be considered for each of the elements analyzed. Specifically, for HE20 element, Fig. 1:

Q1: square section; $\gamma = 1$, $\beta = 0$, $\varepsilon = 1$.

Q2: rectangular section with aspect ratio 1:2; $\gamma = 1/\sqrt{2}$, $\beta = 0$, $\varepsilon = 1$.

Q3: skewed section; $\gamma = 1$, $\beta = 45^{\circ}$, $\varepsilon = 1$.

Q4: distorted in the poling Z-direction with aspect ratio 2:1; $\gamma = 1$, $\beta = 0$, $\varepsilon = 2^{1/3}$.

Q5: distorted in the poling Z-direction with aspect ratio 1:2; $\gamma = 1$, $\beta = 0$, $\varepsilon = 1/2^{1/3}$.

and, for PE15 element, Fig. 2:

T1: triangular section of equilateral geometry; $\gamma = 1$, $\varepsilon = 1$.

T2: triangular section of right geometry; $\gamma^2 = 1/(3)^{1/2}$, $\varepsilon = 1$.

T3: triangular section with angle of 30º opposite to the base; $\gamma^2 = 1/(3)^{1/2}$ tg75º, $\varepsilon = 1$.

T4: distorted in the poling Z-direction with aspect ratio 2:1; $\gamma = 1$, $\varepsilon = 2^{1/3}$.

T5: distorted in the poling Z-direction with aspect ratio 1:2; $\gamma = 1$, $\varepsilon = 1/2^{1/3}$.

Given the mesh and the piezoelectric medium, the dispersion analysis is numerically carried out by a step of $\pi/36$ for the azimuthal and polar angles, and a step of 1/10000 for the dimensionless wave number. As result the indicators Eq. (27), Eq. (30) and Eq. (31), are computed as finite sets of values. An example of the indicators Eq. (30) and Eq. (32) is shown in Fig. 3. It is observed that Eq. (30) and it is deduced that Eq. (31) both vanish as dimensionless wave number goes to zero; that is, as the mesh is refined and in the limit of long waves. It must be remarked that the behavior of the higher order total energy as dimensionless wave number goes to zero is a consequence that both the strain field and the electric field inside each element becomes uniform. That is, given the mesh, in the limit of long waves, the density of total energy

approaches to zero more slowly than its higher order component; and, given the wavelength, as the solution converges on account of mesh refinement, the density of total energy is increasingly dominated by its basic component.

Investigating the relationship between the total energy error and the percentage of higher order total energy Eq. (32), it can be observed from Fig. 3 that both variables could be related by a cubic function for moderate values of the higher order total energy,

$$e_T = \left[A(\phi,\theta,\boldsymbol{\alpha}) * e_h + B(\phi,\theta,\boldsymbol{\alpha})\right] * e_h^2 \tag{34}$$

For each of the waves (SS, FS, and L) and piezoelectric media considered in this research, an averaged correlation between the total energy error and the percentage of higher order total energy is sought by computing averaged values for the coefficients A and B.

First, two reference values of the percentage of higher order total energy are selected,

$$HE20: \quad e_{h1} = 0.10 \quad e_{h2} = 0.20; \quad PE15: \quad e_{h1} = 0.075 \quad e_{h2} = 0.15 \tag{35}$$

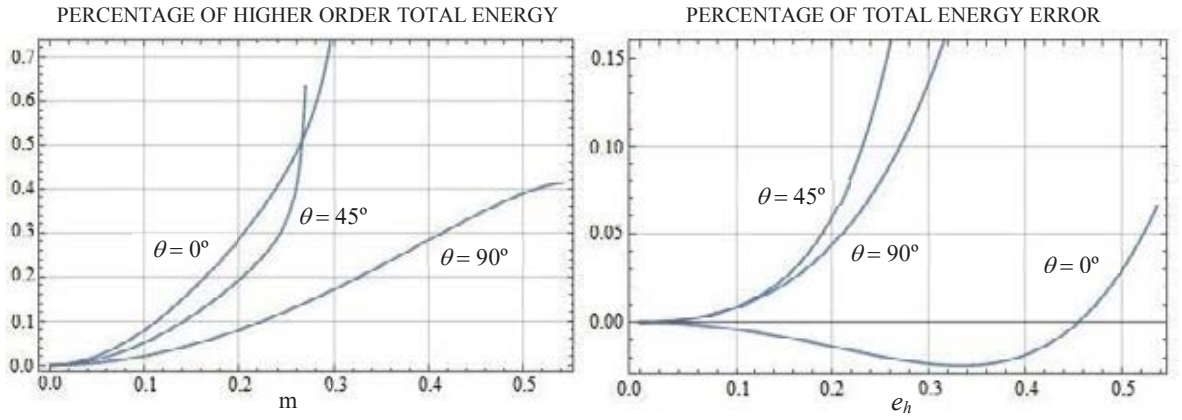

Figure 3: Percentage of higher order total energy versus dimensionless wave number and versus percentage of total energy error. PMN-30PT, MESH Q4, L-WAVES, $\phi = 45°$.

Then, by Eq. (30) and Eq. (32), the reference values related of dimensionless wave number and percentage of total energy error are respectively computed,

$$m_{1,2} = m_{1,2}(\phi,\theta,\boldsymbol{\alpha}), \quad e_{T1,2} = e_{T1,2}(\phi,\theta,\boldsymbol{\alpha}) \tag{36}$$

The mean value of each reference dimensionless wave number, and the root mean square value (based on the L_2-norm) and the sup-norm value [24] of each reference total energy error are next computed on the range of propagation angles,

$$\begin{gathered} m_{1,2}^{M}(\boldsymbol{\alpha}) = \tfrac{1}{\pi^2}\int_0^{\pi}\int_0^{\pi} m_{1,2}\, d\phi d\theta \quad (a) \quad e_{T1,2}^{RMS}(\boldsymbol{\alpha}) = \sqrt{\tfrac{1}{\pi^2}\int_0^{\pi}\int_0^{\pi} \left|e_{1,2}\right|^2 d\phi d\theta} \quad (b) \\ e_{T1,2}^{SUP}(\boldsymbol{\alpha}) = \sup\left\{\left|e_{1,2}(\phi,\theta,\boldsymbol{\alpha})\right|: \quad 0 \le \phi,\theta \le \pi\right\} \quad (c) \end{gathered} \tag{37}$$

Consistent with the discrete analysis carried out, the integrals in Eq. (37a) and Eq. (37b) are numerically computed. Mean values of the indicators of numerical dispersion for the phase velocity and the normal component of the group velocity Eq. (27) have been also computed. Detailed values are presented in the Appendix 2 attached to this manuscript.

As a next step, the values computed in Eq. (37a) and Eq. (37b) are mesh-averaged,

$$HE20: \quad \overline{m_{1,2}^{M}} = \tfrac{1}{5}\sum_{j=1}^{5} m_{1,2}^{M}(Q_j) \qquad PE15: \quad \overline{m_{1,2}^{M}} = \tfrac{1}{5}\sum_{j=1}^{5} m_{1,2}^{M}(T_j) \qquad (a)$$

$$HE20: \quad \overline{e_{T1,2}^{RMS}} = \tfrac{1}{5}\sum_{j=1}^{5} e_{T1,2}^{RMS}(Q_j) \qquad PE15: \quad \overline{e_{T1,2}^{RMS}} = \tfrac{1}{5}\sum_{j=1}^{5} e_{T1,2}^{RMS}(T_j) \qquad (b) \qquad (38)$$

The results of Eq. (38a) and Eq. (38b) are displayed in Table 1 and Table 2, respectively, for each of the piezoelectric media and waves investigated. Similar mesh-averaged values of the indicators of numerical dispersion for the phase velocity and the normal component of the group velocity Eq. (27) have been also computed, Table 3.

From Table 1 and Table 2, it is deduced that the mesh-averaged root mean square values of the first and the second reference percentage of total energy error roughly correspond, in an averaged sense, to six and four elements per wavelength, respectively. In such averaged sense, the total energy error of the quasi-longitudinal waves is greater than the one of the quasi-shear waves. An opposite behavior is shown by the indicators of numerical dispersion. It is deduced from Table 3 that the numerical dispersion of the quasi-shear waves is greater than the one of the quasi-longitudinal waves.

		HE20				HE20	
		PZT-5H	PZT-8	PZT-5A	PMN-30PT	PMN-31PT	PIN-PMN-PT
$\overline{m_1^M}$	SS	0.1758	0.1756	0.1755	0.1751	0.1753	0.1753
	FS	0.1756	0.1758	0.1759	0.1754	0.1754	0.1754
	L	0.1748	0.1749	0.1748	0.1745	0.1745	0.1745
$\overline{m_2^M}$	SS	0.2576	0.2571	0.2567	0.2553	0.2558	0.2557
	FS	0.2568	0.2574	0.2577	0.2564	0.2563	0.2563
	L	0.2542	0.2545	0.2543	0.2530	0.2531	0.2532
		PE15				PE15	
		PZT-5H	PZT-8	PZT-5A	PMN-30PT	PMN-31PT	PIN-PMN-PT
$\overline{m_1^M}$	SS	0.1804	0.1804	0.1802	0.1794	0.1797	0.1797
	FS	0.1804	0.1806	0.1807	0.1803	0.1804	0.1803
	L	0.1797	0.1798	0.1798	0.1796	0.1796	0.1795
$\overline{m_2^M}$	SS	0.2628	0.2627	0.2623	0.2599	0.2607	0.2606
	FS	0.2627	0.2632	0.2634	0.2624	0.2625	0.2624
	L	0.2606	0.2608	0.2607	0.2599	0.2599	0.2598

Table 1: Mesh-average of the mean values of the first and second reference dimensionless wave number.

Finally, by the mesh-averaged reference values of total energy error Eq. (38b), the averaged values of the coefficients A and B for the cubic correlation Eq. (34) can be computed,

$$\overline{e_{T1,2}^{RMS}} = [\overline{A} * e_{h1,2} + \overline{B}] * e_{h1,2}^{2} \qquad (39)$$

Then the averaged correlation between the total energy error and the percentage of higher order total energy will be yielded

$$e_T^{RMS} = (\overline{A} * e_h + \overline{B}) * e_h^2, \quad 0 < e_h \le e_{h2} \qquad (40)$$

3 MODAL ANALYSIS

As application it is explored the use of the averaged correlation Eq. (40) as a reference to apply the higher order total energy as an indicator of discretization error for the finite element vibration eigenmodes. These ones are the solution of the eigenproblem obtained by considering the homogeneous part of Eq. (1) and assuming stationary waves. In condensed form [10],

$$\mathbf{K}^{*}\tilde{\mathbf{x}}_j = \omega_j^2 \mathbf{M}\tilde{\mathbf{x}}_j, \quad \mathbf{K}^{*} = \mathbf{K}_{uu} + \mathbf{K}_{u\phi}\mathbf{K}_{\phi\phi}^{-1}\mathbf{K}_{u\phi}^{T} \quad (a) \quad \tilde{\boldsymbol{\phi}}_j = \mathbf{K}_{\phi\phi}^{-1}\mathbf{K}_{u\phi}^{T}\tilde{\mathbf{x}}_j \quad (b) \quad j = 1,\ldots,n \tag{41}$$

$$\tilde{\mathbf{x}}_i^{T}\mathbf{K}^{*}\tilde{\mathbf{x}}_j = \delta_{ij}\omega_j^2 \quad i,j = 1,\ldots,n \tag{42}$$

where: ω_j and $(\tilde{\mathbf{x}}_j, \tilde{\boldsymbol{\phi}}_j)^T$ are the finite element natural frequencies and eigenvectors.

		HE20				HE20	
		PZT-5H	PZT-8	PZT-5A	PMN-30PT	PMN-31PT	PIN-PMN-PT
$\overline{e_{T1}^{RMS}}$	SS	0.003122	0.002918	0.002759	0.003173	0.003013	0.002986
	FS	0.002698	0.002818	0.003055	0.002731	0.002780	0.002761
	L	0.005648	0.005287	0.005546	0.006690	0.006288	0.006223
$\overline{e_{T2}^{RMS}}$	SS	0.013157	0.012431	0.011570	0.012833	0.012206	0.012081
	FS	0.011348	0.011925	0.012891	0.011663	0.011962	0.011782
	L	0.029571	0.026939	0.028789	0.038235	0.034769	0.034268
		PE15				PE15	
		PZT-5H	PZT-8	PZT-5A	PMN-30PT	PMN-31PT	PIN-PMN-PT
$\overline{e_{T1}^{RMS}}$	SS	0.005515	0.005209	0.005389	0.006292	0.006286	0.006180
	FS	0.005529	0.005393	0.005588	0.005483	0.005412	0.005505
	L	0.007119	0.006555	0.007139	0.008989	0.007935	0.007664
$\overline{e_{T2}^{RMS}}$	SS	0.022301	0.021252	0.021783	0.023798	0.024103	0.023750
	FS	0.022770	0.022237	0.023049	0.022635	0.022367	0.022743
	L	0.033449	0.029710	0.033447	0.052871	0.043976	0.043680

Table 2: Mesh-average of the rms values of the first and second reference percentage of total energy error.

		HE20				HE20	
		PZT-5H	PZT-8	PZT-5A	PMN-30PT	PMN-31PT	PIN-PMN-PT
$\overline{e_{p2}^{M}}$	SS	1.00392	1.00326	1.00342	1.00752	1.00665	1.00654
	FS	1.00356	1.00352	1.00385	1.00321	1.00304	1.00310
	L	1.00194	1.00199	1.00196	1.00168	1.00170	1.00171
$\overline{e_{gn2}^{M}}$	SS	1.01941	1.01614	1.01692	1.03698	1.03269	1.03219
	FS	1.01759	1.01740	1.01902	1.01583	1.01497	1.01525
	L	1.00936	1.00964	1.00947	1.00795	1.00809	1.00815
		PE15				PE15	
		PZT-5H	PZT-8	PZT-5A	PMN-30PT	PMN-31PT	PIN-PMN-PT
$\overline{e_{p2}^{M}}$	SS	1.00386	1.00330	1.00354	1.00640	1.00568	1.00575
	FS	1.00352	1.00339	1.00365	1.00340	1.00322	1.00328
	L	1.00185	1.00191	1.00187	1.00164	1.00167	1.00165
$\overline{e_{gn2}^{M}}$	SS	1.01864	1.01596	1.01708	1.03090	1.02748	1.02783
	FS	1.01718	1.01653	1.01781	1.01652	1.01561	1.01588
	L	1.00897	1.00914	1.00891	1.00673	1.00739	1.00717

Table 3: Second mesh-averaged reference values of the indicators of numerical dispersion.

Eq. (41a) and Eq. (41b) are solved by LAPACK routines [25]. By considering the relation of **K**-orthogonality Eq. (42) for the condensed eigenproblem Eq. (40a), and taking into account Eq. (41b) and Eq. (7), it can be yielded the following expression for the modal total energy

$$\tfrac{1}{4}\tilde{\mathbf{x}}_j^{T}\mathbf{K}_{uu}\tilde{\mathbf{x}}_j + \tfrac{1}{4}\tilde{\boldsymbol{\phi}}_j^{T}\mathbf{K}_{\phi\phi}\tilde{\boldsymbol{\phi}}_j = \tfrac{1}{4}\omega_j^2 \quad \rightarrow \quad \bar{E}_j = \tfrac{1}{4}\omega_j^2, \quad j = 1,\ldots,n \tag{43}$$

The error for the modal total energy computed with the discretized piezoelectric domain is estimated by a reference model that will be obtained by dividing each element of the actual mesh into eight elements. The modal total energy computed with the actual model and the one computed with the reference model will be compared for each eigenmode by

$$TEE = (\bar{E}/\bar{E}^{REF}) - 1, \quad TEE = (\omega/\omega^{REF})^2 - 1 \tag{44}$$

The modal total energy error Eq. (44) will be compared with a proposed total energy error indicator which is computed either by averaging the correlation Eq. (40) for the slow and fast quasi-shear waves, or by the correlation Eq. (40) for the quasi-longitudinal waves,

$$TEES(PHE) = \tfrac{1}{2}(e_{T,SS}^{RMS} + e_{T,FS}^{RMS}) \quad (a) \quad TEEL(PHE) = e_{T,L}^{RMS} \quad (b), \quad 0 < PHE \le e_{h2} \tag{45}$$

where *PHE* is the percentage of higher order total energy computed with the actual model.

From Table 2, the following inequality is clearly fulfilled,

$$TEES(PHE) < TEEL(PHE) \tag{46}$$

Finally, by taking into account Eq. (7), the percentage of modal electric energy will be also computed with the actual model,

$$PEE = \bar{E}^E/(\bar{E}^M + \bar{E}^E) \tag{47}$$

It must be remarked that, for plane bulk acoustic waves, Eq. (47) would be an accepted definition of electromechanical coupling coefficient from energy consideration [26].

3.1 Numerical research

Two test problems discretized by the HE20 element have been analyzed, Fig. 4: a piezoelectric cantilever bimorph connected in parallel configuration made of PZT-5A (L = 16 mm, b = 3 mm, t = 2 mm) [27, 28], and a piezoelectric cube laterally clamped made of PZT-5H or, alternatively, PMN-30PT single crystal (L = 1 mm) [29]. A piezoelectric disk laterally clamped, discretized by the PE15 element, is also analyzed, Fig. 5 (R = 12 mm, t = 6 mm). The piezoelectric disk is made of PZT-8 or, alternatively, PIN-PMN-PT single crystal. In each test problem the electrodes are shorted and their mechanical effects are neglected.

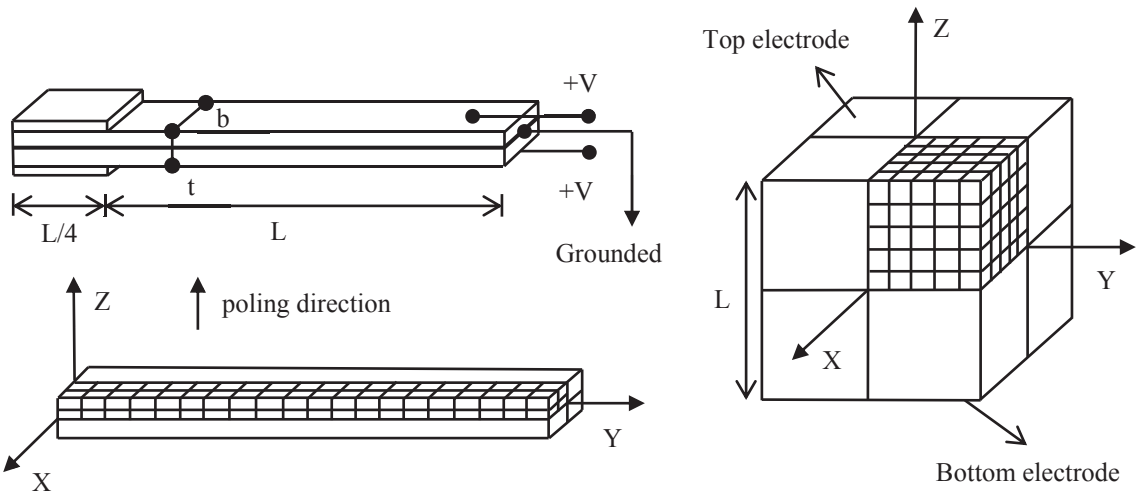

Figure 4: Piezoelectric cantilever bimorph and cube laterally clamped discretized by the HE20 element.

Since the piezoelectric bimorph has two planes of symmetry, which are *XY* and *YZ*, the modes can be computed by idealizing one quarter of it and applying four combinations of boundary conditions on the two planes for symmetric motion (S) and for antisymmetric motion (A), see details in reference [30]. In this test problem, the swaying modes in the Z-direction (AS) and the torsion modes about the Y-axis (AA) have been computed, Table 4.

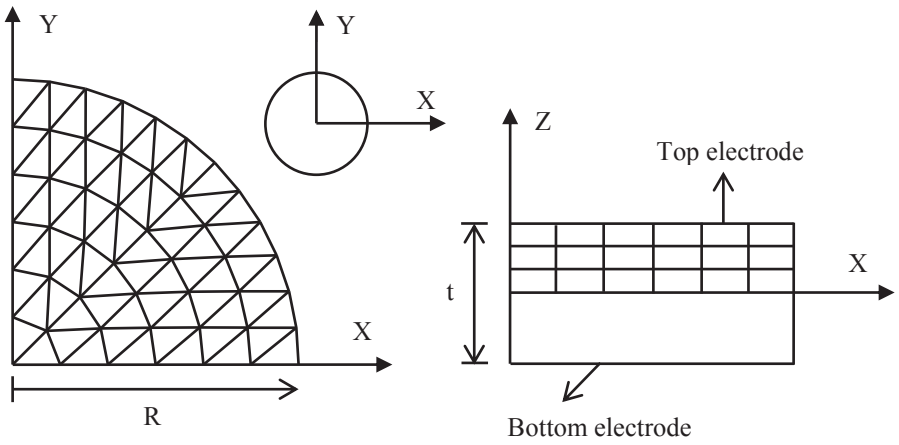

Figure 5: Piezoelectric disk laterally clamped discretized by the PE15 element.

Similarly, since both the piezoelectric cube and the piezoelectric disk have three planes of symmetry, which are *YZ*, *XZ* and *XY*, the modes can be computed by idealizing one eighth of them, and applying six combinations of boundary conditions on the three planes for symmetric motion (S) and for antisymmetric motion (A). Also see details in reference [30]. In both test problems, the antisymmetric and symmetric longitudinal modes in the Z-direction (SSA and SSS), the antisymmetric and symmetric swaying modes in the Y-direction (SAA and SAS), and the antisymmetric and symmetric torsion modes about the Z-axis (AAA and AAS) have been computed. The results are displayed in Tables 5-16.

For each test problem it is selected the set of consecutive eigenmodes for which the following condition is fulfilled: $0 < PHE \leq e_{h2}$ (see Eq. (35)).

#MODE		FR (Hz)	PHE	TEE	TEES	PHE REF	PEE
1	AS	3631.35	0.088188	0.005768	0.002247	0.026710	0.027781
2	AS	21217.95	0.092730	0.005303	0.002490	0.027706	0.031491
3	AA	22773.80	0.139349	0.002560	0.005760	0.039546	0.006289
4	AS	54358.47	0.103447	0.004919	0.003116	0.030374	0.038010
5	AA	68479.08	0.146347	0.002731	0.006376	0.041704	0.008586
6	AS	96273.68	0.120632	0.004907	0.004276	0.034929	0.046683
7	AA	114645.43	0.160009	0.003132	0.007674	0.045951	0.012958
8	AS	143956.67	0.143424	0.005613	0.006114	0.041300	0.056198
8	AA	161540.12	0.179748	0.003882	0.009780	0.052171	0.019010
10	AS	195356.94	0.170984	0.007262	0.008811	0.049380	0.065731
11	AA	209366.65	0.204825	0.005154	0.012858	0.026253	0.060229
12	AS	249168.34	0.201768	0.009994	0.012459	0.074345	0.058857

Table 4: PZT-5A cantilever bimorph. Proposed total energy error indicator TEES versus total energy error computed by mesh halving TEE.

#MODE		FR (Hz)	PHE	TEE	TEES	PHE REF	PEE
1	A	1494798.75	0.044947	0.001012	0.000571	0.012649	0.378348
2	S	2253607.19	0.054692	0.000674	0.000850	0.014552	0.257970
3	A	2911828.99	0.103631	0.002572	0.003131	0.030457	0.160737
4	S	2925280.47	0.104319	0.003437	0.003174	0.031274	0.075176
5	A	2949444.83	0.103972	0.003440	0.003152	0.031517	0.070138
6	S	3219709.13	0.111434	0.002536	0.003635	0.030942	0.194094
7	A	3269260.33	0.132101	0.003350	0.005164	0.037684	0.242467
8	S	3293030.56	0.122009	0.004621	0.004382	0.037425	0.138397
9	S	3343606.11	0.123991	0.003496	0.004530	0.035570	0.043260
10	A	3407876.53	0.106406	0.002466	0.003306	0.029866	0.345914
11	S	3470792.89	0.108399	0.002632	0.003434	0.030465	0.269794
12	A	3546463.33	0.102105	0.001708	0.003037	0.027275	0.170078
13	A	3727337.34	0.127277	0.003860	0.004782	0.035938	0.082845
14	A	3730441.23	0.120325	0.004203	0.004258	0.034218	0.098911
15	S	3785874.14	0.130364	0.002186	0.005024	0.035527	0.050604
16	S	4064314.52	0.163973	0.005918	0.008088	0.050438	0.115876
17	A	4115269.62	0.191198	0.005907	0.011148	0.059473	0.164358
18	S	4218250.54	0.142201	0.004665	0.006015	0.039927	0.084108
19	A	4223091.77	0.165183	0.002378	0.008212	0.045304	0.032168
20	S	4354513.22	0.178546	0.006200	0.009660	0.051740	0.173579
21	S	4440349.35	0.154910	0.005003	0.007185	0.044617	0.090900
22	S	4475618.52	0.170321	0.006235	0.008754	0.047812	0.066334
23	A	4481882.47	0.171154	0.006331	0.008844	0.050257	0.167460
24	A	4530610.59	0.166572	0.005410	0.008357	0.050164	0.293279
25	S	4569360.37	0.204520	0.008802	0.012841	0.059976	0.112327
26	A	4691002.54	0.200371	0.009031	0.012300	0.058179	0.099302
27	A	4755510.15	0.192601	0.005597	0.011321	0.055896	0.129024
28	S	4796773.25	0.170910	0.007932	0.008817	0.052541	0.097511

Table 5: PZT-5H cube laterally clamped. Proposed total energy error indicator TEES versus total energy error computed by mesh halving TEE. Modes SS (S) and SS (A).

#MODE		FR (Hz)	PHE	TEE	TEEL	PHE REF	PEE
1	A	1955083.91	0.047784	0.004777	0.001186	0.014847	0.285874
2	S	2070385.14	0.105834	0.009124	0.007681	0.028318	0.006049
3	S	2347003.92	0.062630	0.002363	0.002204	0.016782	0.332819
4	A	2368802.89	0.113605	0.008700	0.009138	0.032137	0.029402
5	A	2594239.22	0.119986	0.009462	0.010457	0.037010	0.229177
6	S	2904544.18	0.144480	0.013562	0.016629	0.043907	0.180060
7	S	2947810.19	0.169046	0.026569	0.024778	0.055882	0.098489

Table 6: PMN-30PT cube laterally clamped. Proposed total energy error indicator TEEL versus total energy error computed by mesh halving TEE. Modes SS (S) and SS (A).

From Tables 4-16 it is deduced that the percentage of higher order total energy decreases as the mesh is refined. Then, it is verified that this energy component behaves as a modal error indicator, which is in accordance with the numerical dispersion analysis.

From Tables 4, 5, 7, 9, 11, 13 and 15 it can be deduced that, for the solids made of PZT piezoceramics, the proposed total energy error indicator based on S-waves Eq. (45a) and the

total energy error computed by mesh halving Eq. (44) generally exhibit a similar evolution pattern as the modal order increases. Also, the proposed total energy error indicator Eq. (45a) generally overestimates the total energy error computed by mesh halving Eq. (44). Clearly, by the proposed total energy error indicator based on S-waves Eq. (45a), the accuracy of the finite element eigenmodes could be confidently verified in order to select a cutoff modal order given an upper bound for the total energy error close to one per cent.

The above behavior for the solids made of PZT piezoceramics could be expected based on the heuristic that, given the natural frequency, both the percentage of higher order total energy and the spatial discretization error should be mainly influenced by the error induced by the slowest quasi-shear waves which have the shortest wavelengths.

#MODE		FR (Hz)	PHE	TEE	TEES	PHE REF	PEE
1	S	1940056.24	0.037057	0.001392	0.000386	0.011346	0.131090
2	A	2089555.22	0.037879	0.000869	0.000404	0.010915	0.195819
3	A	2434954.09	0.079598	0.002009	0.001824	0.023051	0.374945
4	S	2487876.85	0.069741	0.001248	0.001393	0.019433	0.238560
5	S	2828993.11	0.080055	0.001657	0.001845	0.021692	0.044895
6	A	2982767.69	0.088200	0.001334	0.002250	0.023570	0.057256
7	S	3140640.11	0.090835	0.001926	0.002389	0.025225	0.186659
8	A	3297569.35	0.102153	0.002622	0.003040	0.029069	0.188117
9	S	3421891.52	0.123931	0.002632	0.004526	0.035635	0.075841
10	A	3467280.17	0.139115	0.003948	0.005748	0.041684	0.124472
11	S	3612688.32	0.126168	0.003720	0.004696	0.036407	0.106855
12	A	3775918.50	0.141560	0.003737	0.005959	0.040244	0.174574
13	S	3780264.69	0.128603	0.002931	0.004885	0.036160	0.190129
14	S	3901737.88	0.164548	0.005014	0.008147	0.047153	0.089534
15	A	3904222.86	0.151162	0.003813	0.006828	0.044073	0.255638
16	A	4005566.29	0.159113	0.003850	0.007596	0.045297	0.124791
17	S	4136640.68	0.181068	0.006140	0.009948	0.053140	0.203126
18	A	4178781.08	0.155419	0.003933	0.007234	0.044197	0.193035
19	A	4228182.19	0.167523	0.004781	0.008457	0.047798	0.067265
20	S	4249965.73	0.187775	0.007818	0.010734	0.057300	0.198316
21	S	4364136.58	0.167402	0.005350	0.008444	0.046784	0.079209
22	S	4501655.31	0.182042	0.006794	0.010060	0.050711	0.066730
23	A	4540145.24	0.163551	0.005669	0.008044	0.047357	0.312658
24	A	4620112.25	0.190505	0.007098	0.011064	0.052324	0.055107
25	S	4633649.48	0.179765	0.005468	0.009798	0.050850	0.123484
26	S	4688950.56	0.174831	0.005880	0.009245	0.049616	0.161655
27	A	4758178.95	0.185452	0.006966	0.010458	0.054770	0.122037
28	S	4795991.67	0.195165	0.005529	0.011639	0.056789	0.092402
29	A	4858675.43	0.203334	0.007203	0.012686	0.060966	0.174814

Table 7: PZT-5H cube laterally clamped. Proposed total energy error indicator TEES versus total energy error computed by mesh halving TEE. Modes SA (S) and SA (A).

From Tables 5-16, it can be deduced that the modal total energy errors computed by mesh halving for the solids made of PMN-PT <001> poled single crystals are significantly greater than the ones computed for the solids made of PZT. This behavior is similar to the dilatational locking phenomenon that is most commonly associated with nearly incompressible isotropic materials, i.e., with those for which the Poisson's ratio approaches one-half very closely [13].

From Tables 6, 8, 10, 12, 14 and 16 it can be deduced that, for the solids made of PMN-PT single crystals, only the proposed total energy error indicator based on L-waves Eq. (45b) overestimates for some eigenmodes the total energy error computed by mesh halving Eq. (44); however, by the proposed total energy error indicator based on L-waves Eq. (45b), an upper bound for the total energy error generally can be satisfactorily estimated for the set of eigenmodes selected. Clearly, for the PMN-PT solids, the modal total energy error should be mainly influenced by the error induced by the quasi-longitudinal waves. Both for PMN-30PT cube and for the PIN-PMN-PT disk laterally clamped, the total energy errors computed by mesh halving, for the eigenmodes selected, generally can be accepted for all practical purposes from the engineering point of view.

#MODE		FR (Hz)	PHE	TEE	TEEL	PHE REF	PEE
1	S	1831206.39	0.056366	0.007051	0.001728	0.016903	0.079782
2	A	2215758.70	0.046708	0.004171	0.001126	0.014119	0.221063
3	S	2405588.22	0.110802	0.012973	0.008594	0.032335	0.076049
4	A	2664535.32	0.117330	0.010324	0.009894	0.034096	0.103798
5	S	2794592.00	0.126270	0.014561	0.011868	0.035678	0.121444
6	S	2949954.65	0.090059	0.009531	0.005195	0.025816	0.179932
7	A	3046735.64	0.097286	0.005731	0.006258	0.028028	0.330363
8	A	3090706.07	0.150862	0.016097	0.018547	0.042078	0.033922

Table 8: PMN-30PT cube laterally clamped. Proposed total energy error indicator TEEL versus total energy error computed by mesh halving TEE. Modes SA (S) and SA (A).

#MODE		FR (Hz)	PHE	TEE	TEES	PHE REF	PEE
1	S	2024859.86	0.044406	0.000407	0.000557	0.011471	0.000216
2	A	2303313.34	0.052876	0.000465	0.000793	0.014074	0.082242
3	S	2724869.55	0.070839	0.002311	0.001438	0.020973	0.147724
4	A	2809855.32	0.062111	0.001722	0.001100	0.018002	0.144506
5	S	2937759.52	0.082856	0.001065	0.001980	0.022996	0.152725
6	S	3039991.26	0.090128	0.001847	0.002352	0.025490	0.190031
7	A	3050295.13	0.112990	0.002373	0.003741	0.032682	0.375057
8	S	3549794.00	0.122028	0.003297	0.004383	0.034450	0.164487
9	A	3617277.27	0.125511	0.001897	0.004646	0.034861	0.136241
10	S	3635257.08	0.129175	0.003529	0.004930	0.034367	0.000358
11	A	3668364.29	0.115199	0.002482	0.003893	0.032078	0.189753
12	A	3765104.77	0.136739	0.003342	0.005546	0.036684	0.015491
13	A	3887782.42	0.136244	0.003633	0.005505	0.037601	0.063732
14	S	3893669.38	0.122578	0.003667	0.004424	0.033558	0.054943
15	S	4121863.35	0.159137	0.003041	0.007599	0.043516	0.038288
16	S	4262559.26	0.157842	0.003452	0.007471	0.044082	0.125908
17	A	4269201.31	0.175189	0.004846	0.009284	0.052109	0.234513
18	S	4270499.91	0.184011	0.007730	0.010289	0.053881	0.049026
19	A	4305152.76	0.191207	0.007863	0.011150	0.057651	0.078252
20	S	4430778.46	0.185779	0.004550	0.010497	0.052688	0.141208
21	S	4452728.08	0.186311	0.005351	0.010560	0.053636	0.169705

Table 9: PZT-5H cube laterally clamped. Proposed total energy error indicator TEES versus total energy error computed by mesh halving TEE. Modes AA (S) and AA (A).

#MODE		FR (Hz)	PHE	TEE	TEEL	PHE REF	PEE
1	S	1696277.98	0.043646	0.001614	0.000966	0.011304	0.000239
2	A	2288255.39	0.051260	0.001024	0.001390	0.013540	0.118416
3	S	2600469.55	0.187436	0.027305	0.032316	0.049783	0.002476
4	S	2835507.34	0.091854	0.011700	0.005447	0.027974	0.036460
5	A	2943475.43	0.191199	0.021385	0.034021	0.052110	0.048119
6	A	3031360.11	0.092986	0.011084	0.005610	0.029612	0.107099
7	S	3437664.02	0.173580	0.041123	0.026517	0.067656	0.032985
8	S	3474206.51	0.106232	0.005290	0.007752	0.023311	0.134139
9	S	3491292.14	0.113828	0.005874	0.009182	0.032752	0.246306

Table 10: PMN-30PT cube laterally clamped. Proposed total energy error indicator TEEL versus total energy error computed by mesh halving TEE. Modes AA (S) and AA (A).

#MODE		FR (Hz)	PHE	TEE	TEES	PHE REF	PEE
1	A	51541.31	0.048021	0.002249	0.002153	0.013658	0.177725
2	A	124164.61	0.068596	0.003176	0.004425	0.019245	0.209649
3	A	136836.01	0.079258	0.003836	0.005929	0.022247	0.215999
4	S	150662.77	0.030442	0.001521	0.000860	0.008708	0.053842
5	S	189790.61	0.030784	0.001357	0.000880	0.008937	0.116753
6	S	194972.83	0.045667	0.002401	0.001946	0.012235	0.029768
7	A	198719.09	0.094287	0.005113	0.008433	0.026825	0.221408
8	A	217589.92	0.072451	0.004112	0.004942	0.020729	0.105793
9	S	229412.09	0.064027	0.004506	0.003849	0.017764	0.023877
10	A	230820.02	0.116057	0.008231	0.012870	0.033558	0.201034
11	A	231941.28	0.099038	0.005996	0.009319	0.027954	0.123675
12	A	251548.75	0.069560	0.003639	0.004551	0.019548	0.035352
13	A	257018.78	0.070986	0.001782	0.004742	0.018867	0.003714
14	A	272961.42	0.134343	0.009464	0.017351	0.039191	0.228955
15	S	273635.96	0.101763	0.006729	0.009848	0.027661	0.070426
16	S	277908.60	0.089192	0.006175	0.007533	0.024691	0.090064
17	A	281742.73	0.080465	0.004068	0.006113	0.022439	0.015318
18	S	287413.21	0.110412	0.003803	0.011627	0.030509	0.175302
19	S	287709.83	0.105576	0.006213	0.010613	0.029050	0.105030
20	S	298220.48	0.104759	0.010929	0.010447	0.029507	0.021874

Table 11: PZT-8 disk laterally clamped. Proposed total energy error indicator TEES versus total energy error computed by mesh halving TEE. Modes SS (S) and SS (A).

#MODE		FR (Hz)	PHE	TEE	TEEL	PHE REF	PEE
1	A	50070.97	0.061813	0.012118	0.004817	0.020158	0.282503
2	S	92783.92	0.043018	0.003907	0.002065	0.011601	0.116988
3	S	122410.01	0.064886	0.011353	0.005408	0.019192	0.183122
4	A	123322.12	0.076182	0.013804	0.007960	0.024150	0.262586
5	A	138967.48	0.086335	0.014515	0.010808	0.026849	0.245642
6	S	146426.59	0.050728	0.005403	0.003024	0.014895	0.390335
7	S	147337.01	0.112765	0.022865	0.021031	0.030776	0.057746
8	S	154795.39	0.081233	0.009450	0.009308	0.022474	0.086916

Table 12: PIN-PMN-PT disk laterally clamped. Proposed total energy error indicator TEEL versus total energy error computed by mesh halving TEE. Modes SS (S) and SS (A).

#MODE		FR (Hz)	PHE	TEE	TEES	PHE REF	PEE
1	A	87719.21	0.058070	0.002506	0.003160	0.016293	0.201956
2	S	99192.21	0.011349	0.000872	0.000119	0.003663	0.084222
3	S	150752.21	0.026183	0.001172	0.000635	0.006924	0.009380
4	A	161484.50	0.081146	0.004074	0.006218	0.022875	0.217459
5	A	181107.96	0.096651	0.005297	0.008868	0.027251	0.225069
6	S	192771.32	0.046451	0.002909	0.002014	0.013028	0.035684
7	A	205686.40	0.044962	0.001804	0.001886	0.012630	0.076821
8	A	232909.21	0.060667	0.001457	0.003452	0.016920	0.054281
9	A	236444.46	0.110036	0.006662	0.011546	0.030906	0.217513
10	S	237038.78	0.075228	0.004841	0.005334	0.020399	0.021474
11	S	239632.74	0.063123	0.004437	0.003740	0.017414	0.059033
12	S	251119.89	0.062182	0.002908	0.003628	0.017460	0.138893
13	A	253819.79	0.071411	0.003699	0.004800	0.020122	0.061200
14	S	264704.16	0.084074	0.007583	0.006682	0.023419	0.021252
15	A	270231.84	0.138254	0.010584	0.018400	0.040243	0.187533

Table 13: PZT-8 disk laterally clamped. Proposed total energy error indicator TEES versus total energy error computed by mesh halving TEE. Modes SA (S) and SA (A).

#MODE		FR (Hz)	PHE	TEE	TEEL	PHE REF	PEE
1	S	76742.94	0.021142	0.003894	0.000423	0.006963	0.223332
2	A	88923.44	0.071038	0.013679	0.006721	0.023099	0.245894
3	S	97133.76	0.035209	0.004302	0.001308	0.009999	0.093410
4	S	125002.91	0.066811	0.008671	0.005800	0.018029	0.027904
5	S	145553.70	0.087838	0.014946	0.011277	0.024319	0.073728
6	A	163712.89	0.079371	0.012223	0.008796	0.024630	0.236595
7	S	167542.09	0.138053	0.030572	0.035242	0.039285	0.027827
8	S	172478.18	0.092090	0.016765	0.012673	0.026622	0.172292
9	A	185128.17	0.091919	0.014160	0.012615	0.028045	0.226468
10	S	188251.10	0.091829	0.012304	0.012584	0.025898	0.216315
11	S	193595.02	0.090701	0.012885	0.012206	0.026752	0.294166

Table 14: PIN-PMN-PT disk laterally clamped. Proposed total energy error indicator TEEL versus total energy error computed by mesh halving TEE. Modes SA (S) and SA (A).

4 CONCLUSIONS

For piezoelectric media discretized either by the energy-orthogonal twenty-node hexahedral finite element or by the energy-orthogonal fifteen-node pentahedral finite element, by a dispersion analysis of plane harmonic bulk waves, an averaged correlation between the percentage of higher order total energy and the total energy error is yielded in each case both for the quasi-longitudinal waves and the quasi-shear waves. The use of such correlations as reference to apply the higher order total energy as an error indicator for the finite element vibration eigenmodes in piezoelectric solids is explored. As noteworthy conclusions:

- For PZT piezoceramics discretized by regular meshes the numerical research reveals that, by the correlation based on quasi-shear waves, the accuracy of the finite element eigenmodes can be confidently verified in order to select a cutoff modal order given an upper bound for the total energy error close to one per cent.

- For PMN-PT <001> poled single crystals a phenomenon similar to the dilatational locking could affect the accuracy of the eigenmodes computed. In this case, the correlation based on the quasi-longitudinal waves will be more accurate than the one based on the quasi-shear waves. An upper bound for the total energy error generally can be satisfactorily estimated for the set of eigenmodes selected.

#MODE		FR (Hz)	PHE	TEE	TEES	PHE REF	PEE
1	S	107006.40	0.009654	0.000537	0.000086	0.002590	0.000000
2	A	124403.79	0.068477	0.003158	0.004409	0.019188	0.213427
3	S	151530.13	0.029858	0.001511	0.000827	0.008527	0.060573
4	S	195671.83	0.045609	0.002416	0.001941	0.012245	0.035823
5	S	196124.61	0.052478	0.002468	0.002575	0.013839	0.000000
6	A	198897.48	0.097682	0.005574	0.009061	0.027787	0.218012
7	A	210858.61	0.043840	0.000851	0.001792	0.011718	0.084750
8	A	222906.51	0.099339	0.006712	0.009377	0.028718	0.208479
9	S	230153.98	0.065812	0.005252	0.004069	0.018289	0.026005
10	A	235937.00	0.076905	0.003900	0.005577	0.021555	0.080925
11	A	267146.81	0.081979	0.001640	0.006348	0.021983	0.051653
12	A	268071.13	0.082903	0.003441	0.006494	0.023966	0.089605
13	A	274323.99	0.125060	0.008319	0.014990	0.035278	0.222572
14	S	275419.64	0.103464	0.007639	0.010186	0.028167	0.058666
15	S	280164.97	0.084483	0.006603	0.006748	0.023722	0.102002
16	S	285448.64	0.117184	0.009301	0.013127	0.032024	0.000010
17	A	285499.46	0.084125	0.004895	0.006690	0.023488	0.039281
18	S	290762.64	0.100089	0.005552	0.009521	0.027868	0.147950
19	S	298812.82	0.103531	0.010995	0.010199	0.029058	0.021948

Table 15: PZT-8 disk laterally clamped. Proposed total energy error indicator TEES versus total energy error computed by mesh halving TEE. Modes AA (S) and AA (A).

#MODE		FR (Hz)	PHE	TEE	TEEL	PHE REF	PEE
1	S	71517.07	0.011112	0.001080	0.000107	0.003099	0.002713
2	S	113223.26	0.065395	0.008555	0.005510	0.017477	0.036065
3	S	124328.82	0.046330	0.005056	0.002450	0.013523	0.078704
4	A	130000.47	0.076123	0.012807	0.007946	0.024218	0.209863
5	S	147607.11	0.102151	0.017659	0.016404	0.028347	0.008013
6	S	150955.83	0.045439	0.004820	0.002342	0.013091	0.207442
7	S	176987.11	0.138696	0.036624	0.035666	0.038798	0.011464
8	S	178151.03	0.122330	0.020303	0.025855	0.033400	0.034825
9	S	195577.92	0.149584	0.036575	0.043366	0.042748	0.047200
10	A	201509.80	0.084117	0.011303	0.010138	0.025406	0.232569
11	S	216241.21	0.102550	0.011888	0.016565	0.029350	0.296416
12	S	216933.95	0.153221	0.033238	0.046159	0.046630	0.033856
16	A	227918.97	0.089985	0.011581	0.011969	0.026235	0.202592
14	S	228379.91	0.132431	0.023074	0.031669	0.038939	0.354035

Table 16: PIN-PMN-PT disk laterally clamped. Proposed total energy error indicator TEEL versus total energy error computed by mesh halving TEE. Modes AA (S) and AA (A).

REFERENCES

[1] F. Fahy, *Sound and structural vibration*. Academic Press, 1985.

[2] H.L. Schreyer, Dispersion of semidiscretized and fully discretized systems. T. Belytschko, T.J.R. Hughes eds. *Computational methods for transient analysis*. Elsevier Science, 1983.

[3] F.J. Brito Castro, An error indicator based on a wave dispersion analysis for the vibration modes of isotropic elastic solids discretized by energy-orthogonal finite elements. *European Journal of Computational Mechanics*, **28**, 171-206, 2019.

[4] M. Kimura, A. Ando (revised by D. Maurya, S. Priya), Lead zirconate titanate-based piezoceramics. K. Uchino ed. *Advances piezoelectric materials*. Woodhead Publishing, 2017.

[5] J. Yang, *Analysis of piezoelectric devices*. World Scientific, 2006.

[6] L. Luo, X. Zhao, H. Luo, Single crystal PZN-PT, PMN-PT, PSN-PT, and PIN-PT-based piezoelectric materials. K. Uchino ed. *Advances piezoelectric materials*. Woodhead Publishing, 2017.

[7] J. Peng, H. Luo, T. He, H. Xu, D. Lin, Elastic, dielectric, and piezoelectric characterization of $0.70Pb(Mg_{1/3}Nb_{2/3})O_3$-$0.30PbTiO_3$ single crystals. *Materials Letters*, **59**, 640-643, 2005.

[8] http://www.trstechnologies.com/Resources.

[9] D. Stanfield, A. Elliot, *Underwater electroacoustic transducers*. Peninsula Publishing, 2017.

[10] H. Allik, T.J.R. Hughes, Finite element method for piezoelectric vibration. *International Journal for Numerical Methods in Engineering*, **2**, 151-157, 1970.

[11] B.D. Zaitsev, I.E. Kuznetsova, The energy density and power flow of acoustic waves propagating in piezoelectric materials. *IEEE Transactions on Ultrasonics, Ferroelectrics, and Frequency Control*, **50**, 1762-1765, 2003.

[12] C.A. Felippa, B. Haugen, C. Militello, From the individual element test to finite element templates: evolution of the Patch Test. *International Journal for Numerical Methods in Engineering*, **38**, 199-229, 1995.

[13] R.H. MacNeal, *Finite elements: their design and performance*. Marcel Dekker, 1994.

[14] B.A. Auld, *Acoustic fields and waves in solids. Volume I*. Krieger Publishing Company, 1990.

[15] M. Okrouhlík, C. Höschl, A contribution to the study of dispersive properties of one-dimensional lagrangian and hermitian elements. *Computers and Structures*, **49**, 779-795, 1993.

[16] Z.-Q. Qu, *Model order reduction techniques: with applications in finite element analysis*. Springer, 2004.

[17] R.A. Horn, C.R. Johnson, *Matrix analysis*. Cambridge University Press, 1992.

[18] R.B. King, *Beyond the quartic equation*. Birkhäuser, 1996.

[19] V. Laude, A. Reinhardt, A. Khelif, Equality of the energy and group velocities of bulk acoustic waves in piezoelectric media. *IEEE Transactions on Ultrasonics, Ferroelectrics, and Frequency Control*, **52**, 1869-1871, 2005.

[20] D. Royer, E. Dieulesaint, *Elastic waves in solids I*. Springer, 2000.

[21] L. Brillouin, *Wave propagation in periodic structures*. Dover Publications, 2003.

[22] J. Barlow, More on optimal stress points-reduced integration, element distortions, and error estimation. *International Journal for Numerical Methods in Engineering*, **28**, 1487-1504, 1989.

[23] M. Kaltenbacher, *Numerical simulation of mechatronic sensors and actuators*. Springer, 2015.

[24] J. N. Reddy, *Applied functional analysis and variational methods in engineering*. Krieger Publishing Company, 1991.

[25] E. Anderson, Z. Bai, C. Bischof, S. Blackford, J. Demmel, J. Dongarra, J. Du Croz, A. Greenbaum, S. Hammarling, A. McKenney, D. Sorensen, *LAPACK user's guide*. Society for Industrial and Applied Mathematics, 1999.

[26] B.D. Zaitsev, I.E. Kuznetsova, A.A. Teplykh, Definition of electromechanical coupling coefficient of bulk acoustic waves from energy consideration. *IEEE Symposium on Ultrasonics*, 1467-1470, 2003.

[27] F. Lowrie, M. Cain, M. Stewart, Finite element modelling of electroceramics. NPL Report CMMT(A)150, 1999.

[28] M.S. Vijaya, *Piezoelectric materials and devices*. CRC Press, 2013.

[29] A. Loussert, J-C. Debus, G. Vanderborck, Studying the behavior of piezoelectric single crystals for sonar using ATILA. K. Uchino ed. *Applications of ATILA FEM software to smart materials*. Woodhead Publishing, 2013.

[30] M. Petyt, *Introduction to finite element vibration analysis*. Cambridge University Press, 2010.

Appendix 1. Materials constants for selected piezoelectric media.

C_{IJ}^{E} (GPa)	PZT-5H	PZT-8	PZT-5A	PMN-30PT	PMN.31PT	PIN-PMN-PT
11	126.0	137.0	121.0	160.4	124.0	119.0
12	79.1	69.9	75.9	149.6	111.0	105.0
13	83.9	71.1	75.4	124.0	104.0	104.0
22	126.0	137.0	121.0	160.4	124.0	119.0
23	83.9	71.1	75.4	124.0	104.0	104.0
33	117.0	123.0	111.0	120.0	108.0	114.0
44	23.0	31.3	21.1	53.8	63.0	66.0
55	23.0	31.3	21.1	53.8	63.0	66.0
66	23.5	33.6	22.6	28.7	35.0	25.0
$\varepsilon_{ij}^{S} x10^{8}$ (C/Vm)	PZT-5H	PZT-8	PZT-5A	PMN-30PT	PMN.31PT	PIN-PMN-PT
11	1.505	0.797	0.811	4.394	1.186	1.062
22	1.505	0.797	0.811	4.394	1.186	1.062
33	1.302	0.514	0.735	1.227	0.806	0.645
e_{iJ} (C/m^2)	PZT-5H	PZT-8	PZT-5A	PMN-30PT	PMN.31PT	PIN-PMN-PT
15	17.00	10.40	12.30	31.84	10.30	6.90
24	17.00	10.40	12.30	31.84	10.30	6.90
31	-6.50	-4.00	-5.40	-5.22	-3.90	-4.80
32	-6.50	-4.00	-5.40	-5.22	-3.90	-4.80
33	23.30	13.20	15.80	30.40	22.30	18.60
ρ (kg/m^3)	7500	7600	7750	7740	7740	8000

Table A1.1: Material constants for PZT piezoceramics and PMN-PT <001> poled single crystals.

Appendix 2. Detailed results of the numerical dispersion analysis carried out for media and meshes selected.

				HE20			HE20
m_1^M		PZT-5H	PZT-8	PZT-5A	PMN-30PT	PMN-31PT	PIN-PMN-PT
M-Q1	SS	0.1802	0.1800	0.1799	0.1796	0.1798	0.1798
	FS	0.1799	0.1801	0.1802	0.1797	0.1797	0.1797
	L	0.1791	0.1791	0.1791	0.1788	0.1788	0.1788
M-Q2	SS	0.1756	0.1754	0.1753	0.1749	0.1751	0.1751
	FS	0.1753	0.1755	0.1756	0.1752	0.1751	0.1752
	L	0.1745	0.1745	0.1745	0.1742	0.1742	0.1742
M-Q3	SS	0.1710	0.1709	0.1707	0.1703	0.1706	0.1705
	FS	0.1711	0.1713	0.1714	0.1709	0.1709	0.1709
	L	0.1706	0.1707	0.1706	0.1704	0.1704	0.1704
M-Q4	SS	0.1559	0.1557	0.1557	0.1552	0.1554	0.1554
	FS	0.1556	0.1558	0.1558	0.1554	0.1554	0.1554
	L	0.1548	0.1549	0.1548	0.1545	0.1545	0.1545
M-Q5	SS	0.1963	0.1962	0.1961	0.1956	0.1957	0.1957
	FS	0.1961	0.1962	0.1963	0.1960	0.1959	0.1960
	L	0.1951	0.1952	0.1952	0.1948	0.1948	0.1948
				PE15			PE15
m_1^M		PZT-5H	PZT-8	PZT-5A	PMN-30PT	PMN-31PT	PIN-PMN-PT
M-T1	SS	0.1835	0.1834	0.1833	0.1826	0.1829	0.1829
	FS	0.1834	0.1836	0.1837	0.1834	0.1834	0.1833
	L	0.1827	0.1828	0.1828	0.1826	0.1826	0.1825
M-T2	SS	0..1804	0.1804	0.1802	0.1799	0.1803	0.1801
	FS	0.1806	0.1808	0.1808	0.1804	0.1805	0.1804
	L	0.1799	0.1800	0.1800	0.1798	0.1798	0.1798
M-T3	SS	0.1779	0.1778	0.1777	0.1761	0.1766	0.1767
	FS	0.1780	0.1782	0.1782	0.1779	0.1779	0.1779
	L	0.1774	0.1775	0.1774	0.1772	0.1772	0.1772
M-T4	SS	0.1542	0.1541	0.1540	0.1533	0.1535	0.1536
	FS	0.1540	0.1542	0.1542	0.1538	0.1539	0.1538
	L	0.1534	0.1535	0.1535	0.1533	0.1533	0.1532
M-T5	SS	0.2062	0.2061	0.2060	0.2051	0.2053	0.2053
	FS	0.2062	0.2063	0.2064	0.2061	0.2061	0.2061
	L	0.2052	0.2053	0.2052	0.2050	0.2050	0.2049

Table A2.1: Piezoelectric ceramics PZT and PMN-PT <001> poled single crystals. Mean values of the first reference dimensionless wave number computed over the range of azimuthal and polar angles.

		HE20				HE20	
m_2^M		PZT-5H	PZT-8	PZT-5A	PMN-30PT	PMN-31PT	PIN-PMN-PT
M-Q1	SS	0.2642	0.2635	0.2633	0.2620	0.2624	0.2624
	FS	0.2631	0.2638	0.2641	0.2627	0.2626	0.2626
	L	0.2604	0.2607	0.2605	0.2594	0.2594	0.2595
M-Q2	SS	0.2574	0.2569	0.2565	0.2551	0.2555	0.2555
	FS	0.2565	0.2571	0.2574	0.2561	0.2560	0.2560
	L	0.2536	0.2539	0.2537	0.2523	0.2524	0.2525
M-Q3	SS	0.2499	0.2497	0.2490	0.2478	0.2485	0.2484
	FS	0.2502	0.2507	0.2511	0.2495	0.2495	0.2495
	L	0.2484	0.2486	0.2485	0.2477	0.2478	0.2478
M-Q4	SS	0.2287	0.2281	0.2279	0.2265	0.2269	0.2268
	FS	0.2274	0.2282	0.2283	0.2268	0.2269	0.2268
	L	0.2247	0.2252	0.2249	0.2234	0.2237	0.2238
M-Q5	SS	0.2877	0.2873	0.2870	0.2853	0.2856	0.2855
	FS	0.2870	0.2873	0.2878	0.2867	0.2866	0.2867
	L	0.2838	0.2841	0.2839	0.2822	0.2823	0.2823
		PE15				PE15	
m_2^M		PZT-5H	PZT-8	PZT-5A	PMN-30PT	PMN-31PT	PIN-PMN-PT
M-T1	SS	0.2675	0.2672	0.2669	0.2647	0.2655	0.2655
	FS	0.2671	0.2676	0.2678	0.2668	0.2669	0.2668
	L	0.2650	0.2652	0.2651	0.2645	0.2644	0.2643
M-T2	SS	0.2625	0.2624	0.2619	0.2608	0.2619	0.2614
	FS	0.2629	0.2634	0.2636	0.2624	0.2625	0.2624
	L	0.2610	0.2612	0.2611	0.2603	0.2603	0.2603
M-T3	SS	0.2589	0.2588	0.2583	0.2544	0.2554	0.2557
	FS	0.2591	0.2597	0.2598	0.2589	0.2589	0.2588
	L	0.2572	0.2575	0.2573	0.2569	0.2569	0.2568
M-T4	SS	0.2246	0.2244	0.2242	0.2222	0.2228	0.2228
	FS	0.2240	0.2245	0.2246	0.2234	0.2236	0.2234
	L	0.2222	0.2225	0.2223	0.2214	0.2216	0.2215
M-T5	SS	0.3007	0.3005	0.3001	0.2972	0.2980	0.2978
	FS	0.3005	0.3009	0.3012	0.3004	0.3004	0.3004
	L	0.2974	0.2978	0.2976	0.2965	0.2964	0.2961

Table A2.2: Piezoelectric ceramics PZT and PMN-PT <001> poled single crystals. Mean values of the second reference dimensionless wave number computed over the range of azimuthal and polar angles.

		HE20				HE20	
e_{T1}^{RMS}		PZT-5H	PZT-8	PZT-5A	PMN-30PT	PMN-31PT	PIN-PMN-PT
M-Q1	SS	0.003111	0.002951	0.002747	0.002781	0.002615	0.002589
	FS	0.002440	0.002590	0.002839	0.002930	0.002996	0.002967
	L	0.005436	0.005160	0.005353	0.006342	0.006091	0.006031
M-Q2	SS	0.003213	0.003019	0.002903	0.003171	0.003015	0.003008
	FS	0.002519	0.002608	0.002856	0.002773	0.002799	0.002787
	L	0.005893	0.005474	0.005792	0.007055	0.006668	0.006613
M-Q3	SS	0.003109	0.002987	0.002823	0.002940	0.002816	0.002774
	FS	0.002493	0.002586	0.002803	0.002673	0.002728	0.002738
	L	0.004525	0.004330	0.004461	0.005224	0.004918	0.004890
M-Q4	SS	0.003788	0.002963	0.002673	0.004246	0.003890	0.003829
	FS	0.003075	0.003603	0.004038	0.002462	0.002583	0.002598
	L	0.006038	0.005626	0.005959	0.007375	0.006487	0.006303
M-Q5	SS	0.002391	0.002670	0.002647	0.002729	0.002731	0.002728
	FS	0.002962	0.002702	0.002738	0.002819	0.002793	0.002717
	L	0.006349	0.005853	0.006163	0.007449	0.007278	0.007277
		PE15				PE15	
e_{T1}^{RMS}		PZT-5H	PZT-8	PZT-5A	PMN-30PT	PMN-31PT	PIN-PMN-PT
M-T1	SS	0.005204	0.004864	0.005081	0.005872	0.005807	0.005738
	FS	0.004828	0.004707	0.004887	0.004947	0.004918	0.005011
	L	0.006325	0.005857	0.006344	0.007948	0.007223	0.006921
M-T2	SS	0.005582	0.005380	0.005476	0.006839	0.006869	0.006442
	FS	0.005509	0.005401	0.005555	0.005756	0.005776	0.005813
	L	0.006614	0.006188	0.006638	0.010839	0.009606	0.008615
M-T3	SS	0.005859	0.005642	0.005765	0.005729	0.005891	0.005936
	FS	0.006131	0.005981	0.006151	0.006018	0.005922	0.006063
	L	0.009322	0.008403	0.009355	0.009636	0.008012	0.008553
M-T4	SS	0.004190	0.003745	0.003880	0.004819	0.004663	0.004619
	FS	0.003617	0.003699	0.003907	0.003422	0.003417	0.003452
	L	0.005639	0.005138	0.005625	0.007236	0.006429	0.006180
M-T5	SS	0.006740	0.006416	0.006742	0.008203	0.008201	0.008165
	FS	0.007562	0.007175	0.007438	0.007272	0.007028	0.007186
	L	0.007694	0.007187	0.007731	0.009288	0.008404	0.008053

Table A2.3: Piezoelectric ceramics PZT and PMN-PT <001> poled single crystals. Root-mean-square values of the first reference percentage of total energy error computed over the range of azimuthal and polar angles.

		HE20				HE20	
e_{T2}^{RMS}		PZT-5H	PZT-8	PZT-5A	PMN-30PT	PMN-31PT	PIN-PMN-PT
M-Q1	SS	0.013381	0.012952	0.011943	0.011387	0.010701	0.010581
	FS	0.010521	0.011113	0.012135	0.012881	0.013263	0.013028
	L	0.026983	0.025343	0.026457	0.032994	0.031433	0.031055
M-Q2	SS	0.013659	0.013025	0.012411	0.012765	0.012112	0.012084
	FS	0.010365	0.010741	0.011795	0.011805	0.012004	0.011841
	L	0.031094	0.027931	0.030371	0.040943	0.037724	0.037389
M-Q3	SS	0.013164	0.012886	0.011972	0.011998	0.011539	0.011337
	FS	0.010731	0.011173	0.012022	0.011668	0.012057	0.012025
	L	0.022453	0.021275	0.022036	0.027481	0.025402	0.025162
M-Q4	SS	0.015347	0.011635	0.009988	0.017049	0.015701	0.015482
	FS	0.012378	0.014993	0.016828	0.009974	0.010623	0.010723
	L	0.033683	0.030260	0.032918	0.047561	0.037925	0.036204
M-Q5	SS	0.010234	0.011658	0.011535	0.010967	0.010975	0.010923
	FS	0.012743	0.011603	0.011675	0.011987	0.011861	0.011295
	L	0.033641	0.029885	0.032162	0.042194	0.041363	0.041531
		PE15				PE15	
e_{T2}^{RMS}		PZT-5H	PZT-8	PZT-5A	PMN-30PT	PMN-31PT	PIN-PMN-PT
M-T1	SS	0.021343	0.020127	0.020836	0.022352	0.022299	0.022229
	FS	0.019872	0.019338	0.020127	0.020431	0.020349	0.020722
	L	0.028526	0.025765	0.028627	0.039510	0.034663	0.032725
M-T2	SS	0.021951	0.021364	0.021493	0.025771	0.026720	0.024810
	FS	0.022818	0.022377	0.023026	0.023755	0.023791	0.023963
	L	0.030466	0.028074	0.030559	0.043109	0.037112	0.035260
M-T3	SS	0.023094	0.022519	0.022695	0.020830	0.021604	0.021877
	FS	0.025246	0.024654	0.025354	0.024875	0.024519	0.025062
	L	0.044886	0.038575	0.045003	0.094928	0.073876	0.079793
M-T4	SS	0.017826	0.015975	0.016563	0.018830	0.018301	0.018200
	FS	0.014637	0.015075	0.015944	0.013936	0.013951	0.014109
	L	0.028755	0.025083	0.028547	0.040516	0.033460	0.031638
M-T5	SS	0.027293	0.026275	0.027327	0.031205	0.031590	0.031633
	FS	0.031278	0.029741	0.030795	0.030180	0.029226	0.029860
	L	0.034614	0.031055	0.034500	0.046293	0.040770	0.038983

Table A2.4: Piezoelectric ceramics PZT and PMN-PT <001> poled single crystals. Root-mean-square values of the second reference percentage of total energy error computed over the range of azimuthal and polar angles.

		HE20				HE20	
e_{T1}^{SUP}		PZT-5H	PZT-8	PZT-5A	PMN-30PT	PMN-31PT	PIN-PMN-PT
M-Q1	SS	0.004946	0.005104	0.004941	0.004871	0.004458	0.004589
	FS	0.004842	0.005008	0.004932	0.004646	0.004730	0.004652
	L	0.010287	0.009793	0.010192	0.011434	0.010889	0.010801
M-Q2	SS	0.006064	0.005429	0.006061	0.007097	0.006597	0.006802
	FS	0.004773	0.004942	0.005058	0.004894	0.005017	0.005071
	L	0.011419	0.010569	0.011289	0.012986	0.012092	0.011983
M-Q3	SS	0.006280	0.006588	0.006278	0.006705	0.006410	0.006537
	FS	0.007473	0.007473	0.007473	0.007473	0.007473	0.007473
	L	0.012429	0.011731	0.012293	0.013516	0.012878	0.012787
M-Q4	SS	0.006267	0.005117	0.004463	0.006485	0.005851	0.005693
	FS	0.005446	0.005645	0.006180	0.004974	0.004977	0.004905
	L	0.012539	0.011542	0.012451	0.014192	0.012454	0.012105
M-Q5	SS	0.004866	0.005098	0.004990	0.005691	0.005962	0.006050
	FS	0.005615	0.005225	0.005453	0.005857	0.005873	0.005952
	L	0.011288	0.010573	0.011035	0.012766	0.012186	0.012215
		PE15				PE15	
e_{T1}^{SUP}		PZT-5H	PZT-8	PZT-5A	PMN-30PT	PMN-31PT	PIN-PMN-PT
M-T1	SS	0.017162	0.016391	0.017158	0.017801	0.018963	0.018396
	FS	0.010875	0.010875	0.010875	0.010875	0.010960	0.011192
	L	0.022223	0.019957	0.022213	0.033930	0.033048	0.030928
M-T2	SS	0.017410	0.017854	0.017448	0.020036	0.021348	0.019359
	FS	0.017457	0.017457	0.017457	0.017457	0.017457	0.017468
	L	0.030500	0.028698	0.030492	0.060299	0.050362	0.046393
M-T3	SS	0.018419	0.018323	0.018417	0.016684	0.017354	0.017172
	FS	0.020527	0.020527	0.020527	0.020527	0.020527	0.020527
	L	0.051384	0.044223	0.051347	0.058955	0.047983	0.053773
M-T4	SS	0.017173	0.016383	0.017168	0.017784	0.018966	0.018397
	FS	0.010875	0.010875	0.010875	0.010875	0.010875	0.010875
	L	0.022248	0.019952	0.022238	0.033900	0.033078	0.030923
M-T5	SS	0.017177	0.016386	0.017172	0.017794	0.018978	0.018397
	FS	0.013150	0.012228	0.012845	0.014029	0.014507	0.014523
	L	0.022229	0.019925	0.022219	0.033913	0.033080	0.030943

Table A2.5: Piezoelectric ceramics PZT and PMN-PT <001> poled single crystals. Sup-norm of the first reference percentage of total energy error computed over the range of azimuthal and polar angles.

		HE20				HE20	
e_{T2}^{SUP}		PZT-5H	PZT-8	PZT-5A	PMN-30PT	PMN-31PT	PIN-PMN-PT
M-Q1	SS	0.023199	0.024125	0.023117	0.020298	0.020892	0.020491
	FS	0.023037	0.023882	0.023467	0.022050	0.022476	0.022309
	L	0.053215	0.050128	0.052505	0.060786	0.057137	0.056547
M-Q2	SS	0.025362	0.024742	0.025350	0.029209	0.027160	0.027970
	FS	0.021637	0.022538	0.022121	0.022383	0.023682	0.024075
	L	0.066331	0.057934	0.065265	0.095463	0.078166	0.083769
M-Q3	SS	0.030076	0.031723	0.030035	0.027694	0.028404	0.028348
	FS	0.038762	0.038762	0.038762	0.038762	0.038762	0.038762
	L	0.068921	0.063519	0.067837	0.079279	0.072882	0.072098
M-Q4	SS	0.026212	0.020792	0.016989	0.026779	0.024285	0.023593
	FS	0.025050	0.025642	0.025882	0.023777	0.023850	0.023456
	L	0.077414	0.067116	0.076350	0.100073	0.075566	0.071586
M-Q5	SS	0.023427	0.024327	0.023882	0.023406	0.024710	0.024995
	FS	0.023853	0.021739	0.022733	0.024290	0.024316	0.024581
	L	0.062078	0.056119	0.060119	0.073130	0.068866	0.069332
		PE15				PE15	
e_{T2}^{SUP}		PZT-5H	PZT-8	PZT-5A	PMN-30PT	PMN-31PT	PIN-PMN-PT
M-T1	SS	0.068776	0.067332	0.068762	0.068879	0.068204	0.068301
	FS	0.045641	0.045641	0.045641	0.045641	0.046194	0.046726
	L	0.109239	0.092908	0.109166	0.217268	0.193448	0.182894
M-T2	SS	0.063741	0.064894	0.063723	0.076098	0.082671	0.075965
	FS	0.076963	0.076963	0.076963	0.076963	0.078231	0.079146
	L	0.193846	0.170351	0.193762	0.211705	0.171666	0.183435
M-T3	SS	0.069605	0.071006	0.069599	0.058999	0.062114	0.062565
	FS	0.084933	0.084933	0.084933	0.084933	0.084933	0.084965
	L	0.249039	0.202924	0.248812	0.735536	0.732378	0.723363
M-T4	SS	0.068788	0.067344	0.068775	0.068894	0.068208	0.068322
	FS	0.045638	0.045638	0.045638	0.045638	0.045638	0.045638
	L	0.109306	0.092869	0.109233	0.217447	0.193475	0.182868
M-T5	SS	0.068803	0.067317	0.068790	0.068830	0.068148	0.068261
	FS	0.055850	0.051635	0.054473	0.060503	0.063464	0.062776
	L	0.109354	0.092874	0.109111	0.217424	0.193497	0.183005

Table A2.6: Piezoelectric ceramics PZT and PMN-PT <001> poled single crystals. Sup-norm of the second reference percentage of total energy error computed over the range of azimuthal and polar angles.

		HE20				HE20	
e_{p2}^{M}		PZT-5H	PZT-8	PZT-5A	PMN-30PT	PMN-31PT	PIN-PMN-PT
M-Q1	SS	1.00355	1.00294	1.00301	1.00716	1.00639	1.00624
	FS	1.00337	1.00338	1.00370	1.00299	1.00284	1.00291
	L	1.00195	1.00200	1.00197	1.00169	1.00170	1.00171
M-Q2	SS	1.00359	1.00297	1.00307	1.00724	1.00642	1.00626
	FS	1.00336	1.00335	1.00367	1.00297	1.00282	1.00288
	L	1.00189	1.00194	1.00191	1.00163	1.00164	1.00165
M-Q3	SS	1.00555	1.00464	1.00510	1.00876	1.00757	1.00759
	FS	1.00415	1.00405	1.00438	1.00419	1.00392	1.00398
	L	1.00216	1.00223	1.00218	1.00191	1.00196	1.00195
M-Q4	SS	1.00361	1.00291	1.00292	1.00768	1.00692	1.00690
	FS	1.00360	1.00369	1.00402	1.00310	1.00302	1.00309
	L	1.00202	1.00205	1.00204	1.00170	1.00175	1.00177
M-Q5	SS	1.00332	1.00285	1.00298	1.00674	1.00595	1.00573
	FS	1.00331	1.00315	1.00348	1.00278	1.00258	1.00262
	L	1.00168	1.00175	1.00171	1.00147	1.00146	1.00147
		PE15				PE15	
e_{p2}^{M}		PZT-5H	PZT-8	PZT-5A	PMN-30PT	PMN-31PT	PIN-PMN-PT
M-T1	SS	1.00360	1.00308	1.00327	1.00599	1.00534	1.00540
	FS	1.00335	1.00325	1.00350	1.00326	1.00310	1.00317
	L	1.00185	1.00191	1.00187	1.00167	1.00168	1.00166
M-T2	SS	1.00436	1.00373	1.00405	1.00605	1.00530	1.00557
	FS	1.00367	1.00354	1.00380	1.00377	1.00358	1.00363
	L	1.00194	1.00201	1.00197	1.00176	1.00180	1.00178
M-T3	SS	1.00418	1.00357	1.00387	1.00766	1.00680	1.00667
	FS	1.00361	1.00348	1.00373	1.00346	1.00327	1.00335
	L	1.00189	1.00197	1.00192	1.00159	1.00164	1.00163
M-T4	SS	1.00292	1.00245	1.00255	1.00539	1.00480	1.00490
	FS	1.00278	1.00278	1.00298	1.00253	1.00248	1.00254
	L	1.00160	1.00163	1.00161	1.00141	1.00145	1.00144
M-T5	SS	1.00423	1.00368	1.00397	1.00690	1.00614	1.00620
	FS	1.00421	1.00390	1.00425	1.00400	1.00367	1.00370
	L	1.00195	1.00205	1.00199	1.00177	1.00177	1.00174

Table A2.7: Piezoelectric ceramics PZT and PMN-PT <001> poled single crystals. Mean values of the second reference value for the indicator of dispersion associated with the phase velocity.

		HE20				HE20	
e_{gn2}^{M}		PZT-5H	PZT-8	PZT-5A	PMN-30PT	PMN-31PT	PIN-PMN-PT
M-Q1	SS	1.01756	1.01453	1.01490	1.03521	1.03136	1.03066
	FS	1.01666	1.01668	1.01828	1.01476	1.01402	1.01433
	L	1.00943	1.00966	1.00953	1.00808	1.00813	1.00821
M-Q2	SS	1.01770	1.01467	1.01515	1.03557	1.03153	1.03078
	FS	1.01661	1.01654	1.01814	1.01465	1.01389	1.01419
	L	1.00909	1.00936	1.00920	1.00768	1.00776	1.00784
M-Q3	SS	1.02754	1.02304	1.02534	1.04321	1.03735	1.03747
	FS	1.02062	1.02006	1.02174	1.02075	1.01938	1.01965
	L	1.01052	1.01090	1.01064	1.00924	1.00950	1.00946
M-Q4	SS	1.01778	1.01434	1.01444	1.03767	1.03389	1.03378
	FS	1.01765	1.01810	1.01971	1.01519	1.01477	1.01510
	L	1.00965	1.00983	1.00973	1.00782	1.00818	1.00831
M-Q5	SS	1.01647	1.01410	1.01479	1.03322	1.02933	1.02828
	FS	1.01642	1.01562	1.01724	1.01381	1.01281	1.01299
	L	1.00812	1.00847	1.00827	1.00695	1.00690	1.00695
		PE15				PE15	
e_{gn2}^{M}		PZT-5H	PZT-8	PZT-5A	PMN-30PT	PMN-31PT	PIN-PMN-PT
M-T1	SS	1.01745	1.01492	1.01584	1.02901	1.02590	1.02623
	FS	1.01639	1.01588	1.01710	1.01585	1.01507	1.01539
	L	1.00885	1.00915	1.00896	1.00785	1.00796	1.00790
M-T2	SS	1.02099	1.01798	1.01945	1.02925	1.02574	1.02701
	FS	1.01789	1.01725	1.01850	1.01825	1.01727	1.01754
	L	1.00928	1.00965	1.00940	1.00832	1.00859	1.00845
M-T3	SS	1.02015	1.01723	1.01862	1.03682	1.03275	1.03211
	FS	1.01760	1.01695	1.01821	1.01680	1.01588	1.01625
	L	1.00894	1.00936	1.00906	1.00271	1.00534	1.00456
M-T4	SS	1.01426	1.01194	1.01243	1.02615	1.02334	1.02384
	FS	1.01358	1.01359	1.01457	1.01237	1.01210	1.01236
	L	1.00764	1.00782	1.00770	1.00658	1.00683	1.00683
M-T5	SS	1.02035	1.01772	1.01908	1.03325	1.02968	1.02997
	FS	1.02045	1.01899	1.02066	1.01931	1.01772	1.01786
	L	1.00922	1.00974	1.00942	1.00818	1.00824	1.00811

Table A2.8: Piezoelectric ceramics PZT and PMN-PT <001> poled single crystals. Mean values of the second reference value for the indicator of dispersion associated with the normal component of the group velocity.